Estuarine, Coastal and Shelf Science 95 (2011) 14–28

Contents lists available at ScienceDirect

Estuarine, Coastal and Shelf Science

journal homepage: www.elsevier.com/locate/ecss

Rates and regulation of nitrogen cycling in seasonally hypoxic sediments during winter (Boknis Eck, SW Baltic Sea): Sensitivity to environmental variables

A.W. Dale*, S. Sommer, L. Bohlen, T. Treude, V.J. Bertics, H.W. Bange, O. Pfannkuche, T. Schorp, M. Mattsdotter, K. Wallmann

IFM–GEOMAR Leibniz Institute of Marine Sciences, Wischhofstrasse 1–3, 24148 Kiel, Germany

ARTICLE INFO

Article history:
Received 30 March 2011
Accepted 19 May 2011
Available online 21 July 2011

Keywords:
denitrification
modelling
anammox
Kiel Bight
nitrogen cycle
hypoxia

ABSTRACT

This study investigates the biogeochemical processes that control the benthic fluxes of dissolved nitrogen (N) species in Boknis Eck – a 28 m deep site in the Eckernförde Bay (southwestern Baltic Sea). Bottom water oxygen concentrations (O_{2-BW}) fluctuate greatly over the year at Boknis Eck, being well-oxygenated in winter and experiencing severe bottom water hypoxia and even anoxia in late summer. The present communication addresses the winter situation (February 2010). Fluxes of ammonium (NH_4^+), nitrate (NO_3^-) and nitrite (NO_2^-) were simulated using a benthic model that accounted for transport and biogeochemical reactions and constrained with ex situ flux measurements and sediment geochemical analysis. The sediments were a net sink for NO_3^- (−0.35 mmol m^{-2} d^{-1} of NO_3^-), of which 75% was ascribed to dissimilatory reduction of nitrate to ammonium (DNRA) by sulfide oxidizing bacteria, and 25% to NO_3^- reduction to NO_2^- by denitrifying microorganisms. NH_4^+ fluxes were high (1.74 mmol m^{-2} d^{-1} of NH_4^+), mainly due to the degradation of organic nitrogen, and directed out of the sediment. NO_2^- fluxes were negligible. The sediments in Boknis Eck are, therefore, a net source of dissolved inorganic nitrogen ($DIN = NO_3^- + NO_2^- + NH_4^+$) during winter. This is in large part due to bioirrigation, which accounts for 76% of the benthic efflux of NH_4^+, thus reducing the capacity for nitrification of NH_4^+. The combined rate of fixed N loss by denitrification and anammox was estimated at 0.08 mmol m^{-2} d^{-1} of N_2, which is at the lower end of previously reported values. A systematic sensitivity analysis revealed that denitrification and anammox respond strongly and positively to the concentration of NO_3^- in the bottom water ($NO_{3\,BW}^-$). Higher O_{2-BW} decreases DNRA and denitrification but stimulates both anammox and the contribution of anammox to total N_2 production ($\%R_{amx}$). A complete mechanistic explanation of these findings is provided. Our analysis indicates that nitrification is the geochemical driving force behind the observed correlation between $\%R_{amx}$ and water depth in the seminal study of Dalsgaard et al. (2005). Despite remaining uncertainties, the results provide a general mechanistic framework for interpreting the existing knowledge of N-turnover processes and fluxes in continental margin sediments, as well as predicting the types of environment where these reactions are expected to occur prominently.

1. Introduction

With a total of 2.1 × 10^7 Tg N, the global oceanic nitrogen (N) reservoir dwarfs that of phosphorus (P) (1 × 10^5 Tg P) (Galloway, 2003; Ruttenberg, 2003). However, only 2% of oceanic N is bioavailable as (mainly) nitrate (NO_3^-), with the remainder present as dinitrogen (N_2), which must be fixed by diazotrophs before it can be assimilated into biomass. Consequently, N limitation is widespread in the ocean, and biological fixation is the major source of bioavailable N with lower, yet significant, contributions from continental runoff and atmospheric fallout (Brandes and Devol, 2002; Gruber, 2008). Current estimates from global isotope modelling indicate that total N sources are not balanced with N losses via water column and sedimentary denitrification and the relatively minor sink of particulate organic nitrogen burial in the seafloor (Brandes and Devol, 2002). The main reason for this discrepancy rests with the rate of sedimentary denitrification which, at perhaps 2–3 times higher than N fixation, is quantitatively the most important process in the marine N cycle (Devol, 1991; Codispoti, 1995; Middelburg et al., 1996; Codispoti et al., 2001; Brandes and Devol, 2002; Thullner et al., 2009). In addition to this 'canonical' denitrification (Brandes and Devol, 2002),

* Corresponding author.
E-mail address: adale@ifm-geomar.de (A.W. Dale).

0272-7714/$ – see front matter © 2011 Elsevier Ltd. All rights reserved.
doi:10.1016/j.ecss.2011.05.016

anammox – the microbially catalyzed oxidation of ammonium (NH_4^+) with nitrite (NO_2^-) to N_2 – may account for up to 25% of total N_2 production in continental shelf sediments where 35–70% of global sedimentary denitrification takes place (Gruber and Sarmiento, 1997; Brandes and Devol, 2002; Thamdrup and Dalsgaard, 2002; Thullner et al., 2009). For these reasons, much effort has been placed in recent years on accurately constraining rates of benthic denitrification and anammox in these settings (e.g. Trimmer and Nicholls, 2009).

The source/sink strength of marine sediments for fixed N depends on the rates of the complex array of regulatory microbially mediated pathways occurring there in addition to environmental variables. Organic-rich sediments on continental shelves with low bottom water oxygen concentrations are well recognised loci of denitrification (Berelson et al., 1996; Middelburg et al., 1996). These areas may provide a negative feedback with productivity cycles and amplify the importance of denitrification as a global sink for reactive N in the oceans. The individual role of high carbon content and low oxygen levels on denitrification is, however, more difficult to isolate and quantify since they often occur simultaneously (Hedges and Keil, 1995). In extreme settings, such as oxygen minimum zones (OMZs) or hypoxic water bodies, the N cycle is often dominated by dissimilatory reduction of nitrate to ammonium (DNRA), a microbial reaction carried out by large sulfide oxidizing bacteria such as *Beggiatoa* and *Thioploca* which can store NO_3^- internally at mM concentrations (Fossing et al., 1995; Schulz and Jørgensen, 2001; Jørgensen and Nelson, 2004). In contrast to denitrification and anammox, DNRA recycles NO_3^- to NH_4^+ and preserves fixed N in the system, potentially leading to large fluxes of NH_4^+ to the water column (Otte et al., 1999). Although these giant bacteria are commonly associated with striking microbial mats, they are widespread in coastal sediments where free sulfide accumulates in the porewater (e.g. Jørgensen and Nelson, 2004). Yet, due to the comparably few studies that have assessed DNRA in direct combination with denitrification, the importance of this process for overall N cycling in marine sediments, especially those in seasonally hypoxic environments, is unclear.

The rate of NO_2^- production and consumption in porewater is a critical factor in the sedimentary N balance since NO_2^- is a reactive intermediate in both the nitrification of NH_4^+ to NO_3^- and in the canonical denitrification of NO_3^- to N_2. Uncoupling of these reactions often leads to accumulation of NO_2^- in the porewater, which can elevate the importance of anammox to total benthic N_2 production (Dalsgaard et al., 2005). These authors observed a correlation between water depth and the relative importance of anammox to total N_2 production, hypothesising that carbon oxidation rate was the principle control on anammox versus denitrification. Sediment reworking by bioturbation and the flushing of burrows by infaunal organisms with overlying seawater (i.e. bioirrigation) can also stimulate coupled nitrification–denitrification and/or direct denitrification from overlying water nitrate and complicates the interpretation of measured fluxes (Aller et al., 1983; Gilbert et al., 2003; Dunn et al., 2009; Bertics et al., 2010). Ultimately, the amount of fixed N that is removed from the seafloor depends on the interplay between the fraction of in situ produced NO_2^- that is nitrified or flushed out of the sediment and the fraction that is denitrified to N_2.

In the present study, we combine ex situ fluxes of dissolved nitrogen species (DIN = NH_4^+, NO_2^-, NO_3^-), porewater analyses, sulphate reduction rate measurements and reaction–transport modelling to identify and quantify the major processes driving the fluxes of DIN to and from the sediment in a shallow water (28 m) seasonally hypoxic channel in the SW Baltic Sea (Boknis Eck in the Eckernförde Bay). A systematic sensitivity analysis on the model output is performed to analyse how key environmental variables including carbon fluxes, irrigation rates and bottom water chemistry, regulate the rates of denitrification, nitrification, anammox, DNRA and the relative contribution of anammox to total N_2 production. Our intention is to provide a mechanistic framework to provide further insight into the known trends of anammox and denitrification (Dalsgaard et al., 2005), thereby highlighting the types of environment where these reactions are expected to occur prominently.

2. Material and methods

2.1. Study site

Boknis Eck is a small channel located at the northern entrance of Eckernförde Bay (54° 31′N, 10° 20′ E) and has a water depth of about 28 m (Fig. 1). From mid March until mid September, vertical mixing is restricted by density stratification of the water column, which leads to pronounced periods of hypoxia during late summer due to microbial respiration of organic material in the bottom waters and sediment (Hansen et al., 1999). Phytoplankton blooms generally occur in autumn (September to November) and spring (March/April), and around 75% and 50% of the total bloom production is deposited on the seabed, respectively (Smetacek, 1984), giving rise to an increase in benthic activity (Graf et al., 1983). Autumn storms and a decrease in surface water temperature cause a mixing of the water column and ventilation of the deeper water layers with increased nutrient concentrations (Hansen et al., 1999). During winter, the oxygen penetration depth into the sediments is higher than in summer yet variable (Graf et al., 1983).

The sediments at the study site in Boknis Eck are classified as fine grained muds (<40 μm) with a carbon content of 3–5 wt.% (Balzer et al., 1986, 1987). With no significant terrestrial runoff, the bulk of organic matter within Eckernförde Bay sediments originates from marine plankton and macroalgal sources (Orsi et al., 1996). Degradation and fermentation of organic matter is sufficiently high to produce free methane gas at Boknis Eck but fluid seepage from groundwater discharge has not been observed (Whiticar, 1982; Schlüter et al., 2000). The dominant fauna in the sediments in winter/spring are the polychaetes *Pectinaria koreni* and *Nephtys ciliate* with recorded abundances of 201–476 and 63–122 individuals m^{-2}, respectively (Graf et al., 1982). Specimens up to 10 cm long were present in the core presented in this paper. Bacterial mats were absent on the surface of Boknis Eck sediments at the time of sampling, but *Beggiatoa* are present below the sediment surface at the redox interface at the top of the sulfide layer (Preisler et al., 2007). In late summer 2010 when the bottom waters become almost anoxic (Hansen et al., 1999), we observed a blackening of the surface sediments and colonization by *Beggiatoa* filaments.

2.2. Sampling and analytical methods

Sediment samples were obtained on 18 and 23 February 2010, prior to the spring bloom input, using a multiple corer (MUC) which retrieved cores with a diameter of 10 cm and a maximal length of ca 35 cm. On 1 July 2010 the sediments were sampled using a gravity core. Upon recovery, the cores were immediately transferred to a cool room (4–8 °C) in the IFM–GEOMAR laboratory. Three MUC cores were obtained on 18 February, two of which were sub–sampled for porewater by squeezing 1–2 cm thick slices using a low pressure squeezer (argon at 1–5 bar), filtered through 0.2 μm cellulose acetate Nuclepore® filters and collected in recipient vessels. The third core was sampled anaerobically using Rhizons®. Two MUC cores were obtained on 23 February, one of which was sub-sampled for porewater by squeezing and

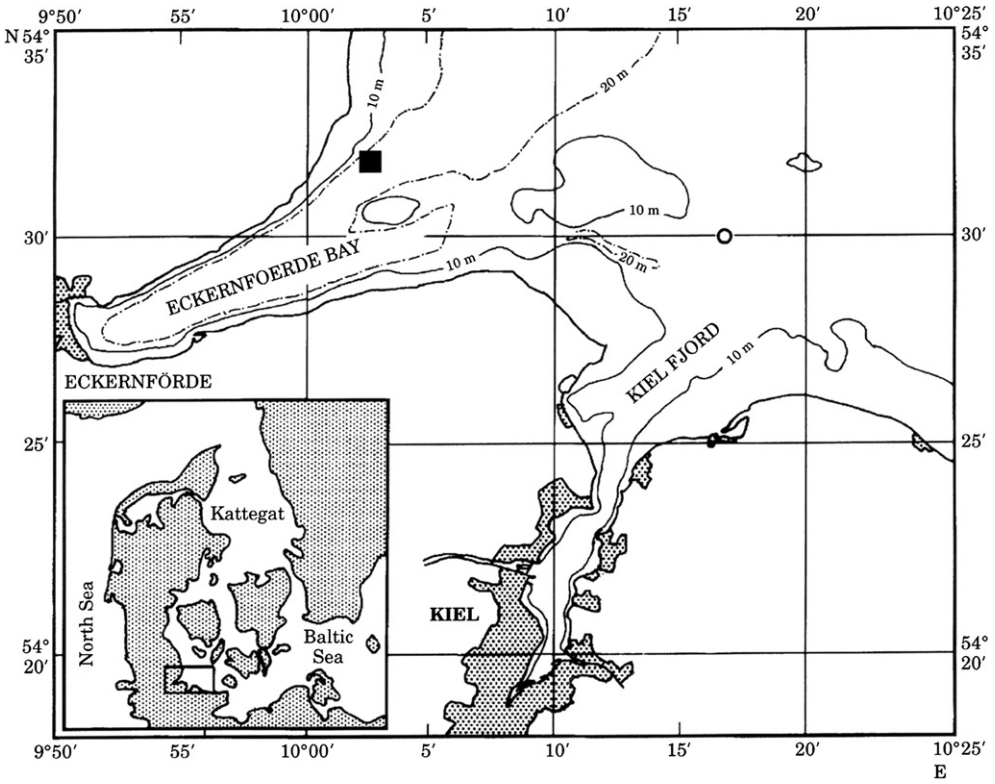

Fig. 1. Location (black square) of the time series station Boknis Eck in the Eckernförde Bay (SW Baltic Sea).

the other using Rhizons. The gravity core was sub-sampled down to 310 cm using Rhizons only. Wet sediment samples (~5 ml) were collected and stored (4–8 °C) for the determination of porosity.

The squeezed porewater samples were analyzed immediately for total alkalinity, nitrate, nitrite, ammonium and sulfide. The porewater sampled using Rhizons was simultaneously analyzed for TA and ammonium and on one occasion sulfide. Porewater TA was determined by titration with 0.02N HCl using the Tashiro indicator, with calibration against IAPSO seawater standard with an accuracy of 0.01 mEq l^{-1}. Nitrate, nitrite, ammonium and sulfide concentrations were analyzed using standard photometric procedures (Grasshoff et al., 1983) on a Hitachi U2800 photometer. Samples for dissolved inorganic carbon determination were acidified to CO_2 with phosphoric acid and measured on a Jena Analytik multi N/C 2100 S analyzer by NDIR analysis. Sulfate concentrations were determined by ion chromatography (Metrohm ion chromatograph with a conventional anion exchange column) using the IAPSO seawater standard for calibration with a relative precision of <5%. There were no obvious differences in the measured concentrations of the samples obtained by Rhizons and squeezed sediments and, therefore, they are not discussed individually.

In this paper, we also present previously published rates of benthic sulfate reduction measured on 5 and 6 March 2002 by Treude et al. (2005). These data are only used to constrain the order of magnitude reactivity of organic carbon because interannual differences in temperature and carbon deposition history can affect the temporal evolution of the rates. Analytical details are presented by these authors.

Concentrations of dissolved oxygen and nutrients in the water column were measured as part of the Boknis Eck Time Series project and determined using standard methods (Hansen, 1999; Hansen and Koroleff, 1999).

In parallel with the porewater and water column studies, sediment cores were taken for incubation experiments. Two MUC cores including overlying water were transferred to the laboratory and incubated at in situ temperature in darkness with a loose fitting lid. The supernatant water was continually circulated using a stirrer ensuring no resuspension of sediment. After 24 h, aliquots were taken from each core at regular intervals for up to 120 h for analysis of nutrients following the methodology described above for porewater. Corrections were made to the flux calculations account for the decrease in water volume with removal of aliquots over the incubation period.

2.3. Model development

2.3.1. Coupling reaction and transport

A steady state reaction–transport model (RTM) was developed for the upper 60 cm of sediments. This depth was chosen in order to capture the main trends in the geochemical profiles in the surface sediment as well as the depth where sulfate reduction ends and methanogenesis begins. In 1–D, the following mass conservation equations (Berner, 1980; Boudreau, 1997) were used to resolve the depth concentration profiles of aqueous, $C_a(z,t)$ and solid, $C_s(z,t)$, species in addition to intracellular nitrate stored in large sulfur bacteria, ($C_b(z,t)$, along the vertical z axis:

$$\varphi(z)\frac{\partial C_a(z,t)}{\partial t} = \frac{\partial}{\partial z}\left(\varphi(z)(D(z)+D_b(z))\frac{\partial C_a(z,t)}{\partial z}\right) - \varphi(z)v_a(z)\frac{\partial C_a(z,t)}{\partial z} + \alpha(z)\varphi(z)(C_a(0,t) - C_a((z,t))) + \varphi(z)\sum R(z,t) \quad (1)$$

$$(1-\varphi(z))\frac{\partial C_s(z,t)}{\partial t} = \frac{\partial}{\partial z}\left((1-\varphi(z))D_b(z)\frac{\partial C_s(z,t)}{\partial z}\right) - (1-\varphi(z))\ v_s(z)\frac{\partial C_s(z,t)}{\partial z} + (1-\varphi(z))\sum R(z,t) \quad (2)$$

$$\varphi(z)\frac{\partial C_b(z,t)}{\partial t} = \alpha_b(z)\varphi(z)(C_b(0,t)-C_b(z,t)) + \varphi(z)\sum R(z,t) \quad (3)$$

where t (d) is time, $\varphi(z)$ is depth-dependent porosity assumed to be at steady state, $v_a(z)$ (cm d^{-1}) and $v_s(z)$ (cm d^{-1}) are the advective or burial velocities of porewater and solids, respectively, $D(z)$ (cm^2 d^{-1}) is the tortuosity corrected molecular diffusion coefficient, $D_b(z)$ (cm^2 d^{-1}) is the biodiffusion coefficient representing sediment mixing by bioturbation, $\alpha(z)$ (d^{-1}) is the depth-dependent bioirrigation coefficient for solutes, $C_a(0,t)$ is the solute concentration at the sediment–water interface, $\alpha_b(z)$ (d^{-1}) is the coefficient for non-local transport of nitrate by filamentous sulfide oxidizing bacteria and $C_b(0,t)$ is the intracellular nitrate concentration at the sediment–water interface. ΣR is the sum of the rate of change of concentration due to biogeochemical reactions. Solute and solid concentrations were modeled in units of mmol cm^{-3} and dry wt.%, respectively. The constitutive equations describing the calculation of the depth-dependent parameters $\varphi(z)$, $D(z)$, $v_s(z)$, $v_a(z)$, $D_b(z)$, $\alpha(z)$ and $\alpha_b(z)$ and corresponding parameters are detailed in the Supplementary Material.

In addition to the above model, hereafter referred to as the 'short core', we developed a second model for the sediments extending from the base of the bioturbation and bioirrigation layer (ca 10 cm) down to 500 cm. The purpose of this model, hereafter referred to as the 'long core', was to provide additional data on bulk reactivity of pelagic particulate organic matter deposited on the seafloor (POM) as well as determining solute concentrations to be used as the lower boundary conditions of the short core where measured concentrations were absent (see below). This approach was necessary since the burial velocity has changed over time, decreasing from 0.3 to 0.9 cm yr^{-1} in the surface layers to 0.07–0.12 cm yr^{-1} at ca 30 cm depth (Balzer et al., 1987; Nittrouer et al., 1998). We assumed the burial velocity in the long core model was 1.9 × 10^{-4} cm d^{-1} (0.07 cm yr^{-1}), and 1.1 × 10^{-3} cm d^{-1} (0.4 cm yr^{-1}) in the short core model.

The long core model considers the reaction and transport of solutes and upward advection of methane gas ($CH_{4(g)}$) using Eq. (4) and (5), respectively:

$$\frac{\partial C_a(z,t)}{\partial t} = \frac{\partial}{\partial z}\left(D\frac{\partial C_a(z,t)}{\partial z}\right) - \omega\frac{\partial C_a(z,t)}{\partial z} + \sum r(z,t) \quad (4)$$

$$\frac{\partial CH_{4(g)}(z,t)}{\partial t} = -\omega_g\frac{\partial CH_{4(g)}(z,t)}{\partial z} + \sum r(z,t) \quad (5)$$

where ω (cm d^{-1}) is the sediment burial velocity and ω_g (cm d^{-1}) is the gas advection velocity, defined as:

$$\omega_g = \omega - \omega_{g0} \quad (6)$$

where ω_{g0} (cm d^{-1}) is the gas advection velocity at the sediment surface determined from model simulations of gassy sediments in Eckernförde Bay (Mogollón et al., 2009). The above equations assume constant porosity, which is justified based on measurements in the gravity core, and that the small gas concentrations predicted by the model do not significantly affect the transport of solutes (Mogollón et al., 2009). Model parameter values are listed in the Supplementary Material.

The short and long core models are both run to steady state, that is $\partial C_i/\partial t = 0$ in Eq. (1) (for i = a,s,b) and $\partial CH_{4(g)}/\partial t = 0$ for $CH_{4(g)}$. This assumption is discussed in 3.2. POC and PON mineralization.

2.3.2. Reaction network and parameterization

Short core. Solutes considered were oxygen (O_2), sulfate (SO_4^{2-}), total hydrogen sulfide (TH_2S), total alkalinity (TA), total dissolved carbon dioxide (TCO_2), nitrate (NO_3^-), intracellular nitrate stored within large sulfur bacteria ($NO_{3\,bac}^-$), nitrite (NO_2^-), dinitrogen (N_2), ammonium (NH_4^+) and dissolved methane (CH_4). The only solid species reported in this study is POM. However, the model also includes the phosphorus and iron cycles including dissolved ferric iron (Fe^{2+}) and solid reactive iron oxide ($Fe(OH)_3$). Since the focus of was on the benthic nitrogen cycle, their discussion is reserved for a separate manuscript. The reaction network and relevant conversion factors for simulating mixed phase reactions are detailed in Table 1 and kinetic parameters are listed in Table 2.

The chemical reactions are ultimately driven by the degradation of POM, considered here to occur by aerobic respiration, denitrification, dissimilatory iron reduction, sulfate reduction and methanogenesis. Three reactive POM pools (Gi) were considered; a fast reacting pool ($i = 1$) which decays in the 10 cm upper mixed layer and two additional pools of lower reactivity (G2 and G3) which decay over much longer time scales. In the model, POM is chemically defined as $CH_2O(NH_3)_{(N:C)i}$ where $(N:C)_i$ is the mineralization ratio of particulate organic nitrogen (PON, assumed equivalent to NH_3) to particulate organic carbon (POC, defined chemically as CH_2O) in pool i = 1, 2, 3. POM degradation is described by first order kinetics using individual rate constants, k_{Gi}, for each pool. The rate of POM mineralization at each depth by each pathway is determined by concentration of electron acceptors existing at that specific depth using Michaelis Menten kinetic limitation terms (f_j, Table 1). Mineralization liberates TCO_2 and NH_4^+ to the porewater according to the N:C ratio of the POM. Ammonification is a term used here to describe the release of inorganic nitrogen as NH_4^+ during POM mineralization. The reduced metabolites of POM mineralization (NH_4^+, Fe^{2+}, H_2S, CH_4) were allowed to leave the sediment by diffusion, burial and irrigation or be oxidized.

The first order rate constants which define POM reactivity were constrained from the measured data. The reactivity of G1 was primarily obtained by simulating the fluxes and concentrations of NH_4^+ and the sulfate reduction rates measured ex situ using $^{35}SO_4^{2-}$ (Treude et al., 2005). A better simulation of the data was obtained by allowing enhanced degradation of organic matter by aerobic versus anaerobic respiration pathways (e.g. Hedges and Keil, 1995), prescribed using the factor, (f_{ox}, Table 1). The reactivity of G2 and G3 was extracted by modeling SO_4^{2-}, TA, TCO_2 and NH_4^+ concentrations in the long core (see Supplementary Material). Ex situ NH_4^+ fluxes provided a further check on total POM degradation.

Canonical denitrification was modeled as a two step process, $NO_3^- \rightarrow NO_2^- \rightarrow N_2$ (R_{NO3}, R_{NO2}), with NO_2^- as an intermediate species (Table 1). For simplicity, these reactions are referred to as step 1 and step 2 of denitrification, although step 1 is not a denitrifying (N_2 producing) reaction. The kinetics of this process was formulated such that POM degradation via NO_3^- was inhibited by the accumulation of NO_2^- due to greater catabolic energy yields for the second step under standard conditions, i.e. POM was preferentially degraded by NO_2^- before NO_3^-. The formation of nitrous oxide (N_2O) during the intermediate steps of denitrification was not considered. Nitrification is described as the stepwise oxidation of $NH_4^+ \rightarrow NO_2^- \rightarrow NO_3^-$ (R_{NH4ox}, R_{NO2ox}) since it requires the intervention of 2 bacteria (e.g. *Nitrosomonas* and *Nitrobacer* spp.). Nitrification competes for NO_2^- with denitrification (R_{NO2}) and anammox (R_{amx}). Due to the presence of *Beggiatoa*, DNRA is also

Table 1
Reaction networks used in the models. Rates of POM degradation are dependent on the specific pool, Gi, under consideration. For the short core, $i = 1, 2, 3$, and for long core, $i = 2, 3$. Porewater species are in mmol cm^{-3} of porewater and solid phase species in dry wt.%. Gi is defined as $CH_2O(NH_3)_{(N:C)i}$.

Rate	Stoichiometry	Rate expression[a]	Unit
Short core			
R_{O2}	$G_i + O_2 \rightarrow (N:C)_iNH_4^+ + (1-(N:C)_i)CO_2 + (N:C)_iHCO_3^- + (1-(N:C)_i)H_2O$	$k_{Gi}\cdot f_{ox}\cdot G_i/f_{POC}\cdot f_{O2}$	mmol cm^{-3} d^{-1} of TCO_2
R_{NO3}	$G_i + 2NO_3^- \rightarrow 2NO_2^- + (N:C)_iNH_4^+ + (1-(N:C)_i)CO_2 + (N:C)_iHCO_3^- + (1-(N:C)_i)H_2O$	$k_{Gi}\cdot G_i/f_{POC}\cdot f_{NO3}\cdot(1-f_{NO2})\cdot(1-f_{O2})$	mmol cm^{-3} d^{-1} of TCO_2
R_{NO2}	$G_i + 1.33NO_2^- + (1.33 + (N:C)_i)CO_2 \rightarrow 0.66N_2 + (N:C)_iNH_4^+ + (1.33 + (N:C)_i)HCO_3^- + (1.33-(N:C)_i)H_2O$	$k_{Gi}\cdot G_i/f_{POC}\cdot f_{NO2}\cdot(1-f_{O2})$	mmol cm^{-3} d^{-1} of TCO_2
R_{Fe}	$G_i + 4Fe(OH)_3 + (1 + (N:C)_i)CO_2 \rightarrow 4Fe^{2+} + (8 + (N:C)_i)HCO_3^- + (N:C)_iNH_4^+ + (3-(N:C)_i)H_2O$	$k_{Gi}\cdot G_i/f_{POC}\cdot f_{Fe}\cdot(1-f_{NO3})\cdot(1-f_{NO2})\cdot(1-f_{O2})$	mmol cm^{-3} d^{-1} of TCO_2
R_{SO4}	$G_i + 0.5SO_4^{2-} + (N:C)_iCO_2 + (N:C)_i\cdot H_2O \rightarrow 0.5H_2S + (N:C)_iNH_4^+ + (1 + (N:C)_i)HCO_3^-$	$k_{Gi}\cdot G_i/f_{POC}\cdot f_{SO4}\cdot(1-f_{Fe})\cdot(1-f_{NO3})\cdot(1-f_{NO2})\cdot(1-f_{O2})$	mmol cm^{-3} d^{-1} of TCO_2
R_{CH4}	$G_i + (N:C)_iH_2O \rightarrow 0.5CH_4 + (N:C)_iNH_4^+ + (0.5-(N:C)_i)CO_2 + (N:C)_iHCO_3^-$	$k_{Gi}\cdot G_i/f_{POC}\cdot(1-f_{SO4})\cdot(1-f_{Fe})\cdot(1-f_{NO3})\cdot(1-f_{NO2})\cdot(1-f_{O2})$	mmol cm^{-3} d^{-1} of TCO_2
R_{DNRA}	$HS^- + NO_3^- + CO_2 + 2H_2O \rightarrow SO_4^{2-} + NH_4^+ + HCO_3^-$	$k_{DNRA}\cdot NO_3^-\cdot TH_2S$	mmol cm^{-3} d^{-1} of NO_3^-
R_{amx}	$NH_4^+ + NO_2^- \rightarrow N_2 + 2H_2O$	$k_{amx}\cdot NO_2^-\cdot NH_4^+$	mmol cm^{-3} d^{-1} of N_2
R_{NH4ox}	$NH_4^+ + 1.5O_2 + 2HCO_3^- \rightarrow NO_2^- + 3H_2O + 2CO_2$	$k_{NH4ox}\cdot O_2\cdot NH_4^+$	mmol cm^{-3} d^{-1} of NH_4^+
R_{NO2ox}	$NO_2^- + 0.5O_2 \rightarrow NO_3^-$	$k_{NO2ox}\cdot O_2\cdot NO_2^-$	mmol cm^{-3} d^{-1} of NO_2^-
R_{H2Sox}	$HS^- + 2O_2 + HCO_3^- \rightarrow SO_4^{2-} + CO_2 + H_2O$	$k_{H2Sox}\cdot O_2\cdot TH_2S$	mmol cm^{-3} d^{-1} of HS^-
R_{AOM}	$CH_4 + SO_4^{2-} \rightarrow HS^- + HCO_3^- + H_2O$	$k_{AOM}\cdot CH_4\cdot SO_4^{2-}$	mmol cm^{-3} d^{-1} of CH_4
Long core			
R_{SO4}	$G_i + 0.5SO_4^{2-} + (N:C)_iCO_2 + (N:C)_iH_2O \rightarrow 0.5H_2S + (N:C)_iNH_4^+ + (1 + (N:C)_i)HCO_3^-$	$R_{Gi}\cdot f_{SO4}$	mmol cm^{-3} d^{-1} of TCO_2
R_{CH4}	$G_i + (N:C)_iH_2O \rightarrow 0.5CH_4 + (N:C)_iNH_4^+ + (0.5-(N:C)_i)CO_2 + (N:C)_iHCO_3^-$	$R_{Gi}\cdot(1-f_{SO4})$	mmol cm^{-3} d^{-1} of TCO_2
R_{AOM}	$CH_4 + SO_4^{2-} \rightarrow HS^- + HCO_3^- + H_2O$	$k_{AOM}\cdot CH_4\cdot SO_4^{2-}$	mmol cm^{-3} d^{-1} of CH_4
R_{GF}	$CH_4 \rightarrow CH_{4(g)}$ if $CH_4 \geq CH_4^*$	$k_{GF}\cdot(CH_4-CH_4^*)$	mmol cm^{-3} d^{-1} of CH_4
R_{diss}	$CH_{4(g)} \rightarrow CH_4$ if $CH_4 < CH_4^*$ and $CH_{4(g)} > 0$	$k_{diss}\cdot(CH_4^*-CH_4)\cdot CH_{4(g)}$	mmol cm^{-3} d^{-1} of CH_4

[a] Methodology for estimating RGi for the long core model is provided in the Supplementary Material.
Conversion factor between POC (dry weight %) and TCO_2 (mmol cm^{-3}): $f_{POC} = 100\%\cdot 12gC/molC\cdot\varphi(z)/(10^3 mmol/mol\cdot\rho_s\cdot(1-\varphi(z)))$.
Kinetic limiting terms: $f_j = [j]/([j]+K_j)$(for $j = O_2, NO_2^-, NO_3^-, Fe(OH)_3, SO_4^{2-}$), where K_j is the half-saturation constant for electron acceptor j.

included (R_{DNRA}). We consider that the major end products of this reaction are SO_4^{2-} and NH_4^+ (Jørgensen and Nelson, 2004).

Denitrification coupled to Fe^{2+} oxidation (Straub et al., 1996) may compete with canonical denitrification for NO_3^-. Abiotic or biotic oxidation of NH_4^+ by metal oxides may also act as an in situ source for NO_3^- which can be denitrified (Hulth et al., 1999). These reactions were not considered in the model due to a lack of data needed to constrain their rates and their relevance remains uncertain at this time. In what follows, the term 'denitrification' applies to canonical denitrification (i.e. R_{NO2} and R_{NO3}) rather than anammox or anaerobic iron oxidation.

Anaerobic oxidation of methane (AOM) is the final reaction considered in the short core model, and was described using bimolecular kinetics (R_{AOM}, Table 1). This expression thus does not explicitly account for reactive intermediates (e.g. hydrogen, acetate) which may be shuttled between methane oxidizers and sulfate reducers (e.g. Dale et al., 2008a), yet it is sufficient to meet the objectives of this study.

Long core. The reaction network for the long core model was a simplified version of the short core model (Table 1). Solutes considered were SO_4^{2-}, TCO_2, NH_4^+ and CH_4. Gaseous methane ($CH_{4(g)}$) was also included since upward transport and dissolution of gas may be an important control on the CH_4 profile and, by extension, on the depth of sulfate penetration (Mogollón et al., 2009).

POM was assumed to be mineralized by sulfate reduction and methanogenesis only since other degradation pathways are mainly confined to the upper 10 cm mixed or bioturbated layer. POM concentrations were not modeled explicitly; instead the rate of POM degradation in the long core model was imposed directly. Two reactive POM pools were considered; G2 and G3 as defined above. The fast reacting G1 pool pertains to the upper mixed layer only. G2 and G3 were assumed to undergo exponential decay with depth (i.e. time) in the sediment (Berner, 1964), which allowed the following degradation rates of these fractions to be formulated on the basis of the carbon containing fraction:

$$R_{G2}(z) = R_{G2}(b)\cdot\exp[-\gamma_{G2}\cdot(z-zb)] \text{ for } z > zb \quad (7)$$

$$R_{G3}(z) = R_{G3}(b)\cdot\exp[-\gamma_{G3}\cdot(z-zb)] \text{ for } z > zb \quad (8)$$

where depth, z, refers to the sediment depth below the bioturbation zone, $R_{Gi}(z)$ (mmol cm^{-3} d^{-1} of C) is the depth-dependent rate of POC mineralization of POM pool $i = 2$ or 3, $R_{Gi}(b)$ is the rate at the base of the bioturbated layer ($z = b$) and γ_{Gi} (cm^{-1}) is the rate attenuation coefficient. The procedure for estimating these parameters is outlined in the Supplementary Material.

The other reactions considered in the long core are AOM and methane gas production and dissolution. The rates of gas formation, R_{GF}, and dissolution, R_{diss}, were described using kinetic expressions of the departure from the local solubility concentration, CH_4^* (Dale et al., 2008b). CH_4^* (mol L^{-1}) depends on salinity, temperature and pressure and was calculated using the algorithm in Dale et al. (2008b).

2.3.3. Boundary conditions and model solution

In the short core, boundary conditions at the top of the sediment for solutes were imposed as fixed concentrations (Dirichlet boundary) using values measured in the bottom water or estimated from the porewater data in the surface sediments. The intracellular nitrate concentration ($NO_{3\,bac}^-$) is unknown, but given that the surface sediments were oxygenated and no surface *Beggiatoa* were observed, the concentration to $NO_{3\,bac}^-$ was set equal to NO_3^-. Concentrations of O_2, NO_3^-, $NO_{3\,bac}^-$, NO_2^-, N_2 and SO_4^{2-} at the bottom ($z = 60$ cm) were specified as a zero gradient (Neumann boundary). Bottom boundaries for TA, TCO_2, TH_2S, NH_4^+ and CH_4 were defined as fixed concentrations determined from the measured data and

Table 2
Parameters used in the reaction network of the short and long core models. (L: based on previously reported values; M: constrained with the model, I: independently determined from data).

Parameter	Description	Value	Unit	Source
Short core				
k_{G1}	Rate constant for G1 degradation	1.4×10^{-4}	d^{-1}	M
k_{G2}	Rate constant for G2 degradation	*From long core*		
k_{G3}	Rate constant for G3 degradation	*From long core*		
f_{ox}	Enhancement factor for aerobic POM degradation	10	1	M
K_{O2}	Half-saturation constant for O_2	1	μM	L[a]
K_{NO3}	Half−saturation constant for NO_3^-	10	μM	L[a]
K_{NO2}	Half−saturation constant for NO_2^-	10	μM	L[a]
K_{Fe}	Half−saturation constant for $Fe(OH)_3$	0.028	wt.%	L[a]
K_{SO4}	Half−saturation constant for sulfate	*From long core*		
k_{NH4ox}	Rate constant for aerobic oxidation of NH_4^+	2.7×10^4	$M^{-1}\ d^{-1}$	L[a]
k_{NO2ox}	Rate constant for aerobic oxidation of NO_2^-	2.7×10^4	$M^{-1}\ d^{-1}$	L[a]
k_{amx}	Rate constant for anammox	2.7×10^4	$M^{-1}\ d^{-1}$	L[a]
k_{DNRA}	Rate constant for DNRA	2.7×10^5	$M^{-1}\ d^{-1}$	L[a]
k_{H2Sox}	Rate constant for aerobic oxidation of TH_2S	2.7×10^4	$M^{-1}\ d^{-1}$	L[a]
k_{AOM}	Rate constant for AOM	*From long core*		
$(N:C)_1$	Molar mineralization ratio of N:C in G1	9.5/106	mol N (mol C)$^{-1}$	M
$(N:C)_2$	Molar mineralization ratio of N:C in G2	*From long core*		
$(N:C)_3$	Molar mineralization ratio of N:C in G3	*From long core*		
Long core				
k_{G2}	Rate constant for G2 degradation	4.1×10^{-6}	d^{-1}	M
k_{G3}	Rate constant for G3 degradation	1.15×10^{-6}	d^{-1}	M
K_{SO4}	Half−saturation constant for sulfate	0.5	mM	L[b]
k_{AOM}	Rate constant for AOM	27.4	$M^{-1}\ d^{-1}$	L[b]
k_{GF}	Rate constant for methane gas formation	0.27	d^{-1}	L[b]
k_{diss}	Rate constant for methane gas dissolution	2.73	$M^{-1}\ d^{-1}$	L[b]
CH_4^*	In situ solubility of methane gas	7	mM	I
$(N:C)_2$	Molar mineralization ratio of N:C in G2	8/106	mol N (mol C)$^{-1}$	M
$(N:C)_3$	Molar mineralization ratio of N:C in G3	27/106	mol N (mol C)$^{-1}$	M

[a] Bohlen et al. (2010).
[b] Dale et al. (2008b).

the steady state results from the long core model. This choice of boundary condition is justified since the concentration and fluxes of these solutes below 60 cm are highly influenced by the mineralization of the G2 and G3 pools (see Section 3.2). Fluxes for solids were imposed at the sediment surface (Robin boundary). The G1 flux was constrained from the measured rates of sulfate reduction whereas fluxes of G2 and G3 were set equal to the respective depth-integrated rates of POC mineralization obtained from the long core. At the bottom solids were specified with a zero gradient.

In the long core, solute boundary conditions at the top of the sediment ($z = b$) were imposed as fixed concentrations using values which were measured (SO_4^{2-}, TA, TCO_2, NH_4^+) or estimated (CH_4). Solute concentrations at the bottom were specified as a zero gradient.

The set of coupled partial differential equations that describes the dynamics of the model variables was transformed using the method of lines by replacing the continuous spatial derivatives in Eq. (1) to (5) with finite differences (Boudreau, 1997). The resulting set of ordinary differential equations was solved using the NDSolve algorithm in MATHEMATICA over an uneven grid of 600 nodes of increasing thickness with depth in the sediment for both the short and long core models. The models were >99% mass conservative.

2.4. System analysis

The reaction−transport model is a highly interconnected biogeochemical system with many potential couplings between reactions. It is our interest to determine which aspects of the parameter set, forcing functions and associated uncertainties, have the most effect on N turnover rates. Taking a stepwise approach involving manually changing parameter values individually and observing the model response change does not identify couplings between parameters. Consequently, a system analysis based on a two level factorial design was applied to the model to determine which parameters and boundary conditions have the most effect on N turnover rates. This statistical methodology monitors the response of a predefined system output or attribute (for example, a reaction rate or concentration) to the perturbations of n model 'factors' (for example, reaction parameters or forcing functions). As described by Box et al. (1978), each factor is assigned a high and low level, and the procedure returns the 'effect' of all possible high and low level factor permutations on the model response. For n factors, there are a total of 2^n permutations and 2^n system responses, meaning that the system must be analyzed 2^n times. Transformed individual and combined parameter effects are subsequently calculated from the vector of system responses using a simple algorithm. Normal probability plots of the transformed affects are used to visualize the factors or factor interactions that have the largest impact on the system response (Box et al., 1978). A previous application of factorial analyses to marine sediment dynamics is given by Dale et al. (2006).

In this study, the identified model responses were the depth integrated rates of DNRA, nitrification, denitrification, anammox and the relative importance of anammox to total N_2 production (% $R_{amx} = R_{amx}/(R_{NO2}+R_{amx}) \times 100\%$)). The set of factors tested were those related to environmental forcings and suspected to have the largest effect on these responses. These include the flux (F_{G1}) and reactivity (k_{G1}) of G1, $D_b(0)$, $\alpha_1(0)$ and $\alpha_{b1}(0)$ in addition to bottom water concentrations of oxygen, nitrate and nitrite (O_{2-BW}, $NO_{3\,BW}^-$ and $NO_{2\,BW}^-$, respectively). The 8 factors require (2^8=) 256 model simulations to fully test the complete array of factor combinations. The high and low factor levels for O_{2-BW}, $NO_{3\,BW}^-$ and $NO_{2\,BW}^-$ were set according the average intra−annual maximum and minimum values in the Boknis Eck time series dataset (Hansen, 1993) (Table 3). The high and low levels of F_{G1}, k_{G1}, $D_b(0)$, $\alpha_1(0)$ and $\alpha_{b1}(0)$ were prescribed to expected variations in this environment. It is

Table 3
Low and high levels of the environmental factors tested in the factorial analysis.

Factor	Low	High	Unit
F_{G1}	9×10^{-4}	2.1×10^{-3}	mmol cm^{-2} d^{-1} of C
k_{G1}	6.9×10^{-5}	2.7×10^{-4}	d^{-1}
$D_b(0)$	2.7×10^{-3}	0.14	cm^2 d^{-1}
$\alpha_1(0)$	0.027	0.27	d^{-1}
$\alpha_{b1}(0)$	0.27	1.37	d^{-1}
O_{2-BW}	5	350	μM
$NO_{3\,BW}^-$	1.5	15	μM
$NO_{2\,BW}^-$	0.1	1	μM

important to remember that the system analysis results may not be universally applicable and are only valid for the specific ranges over which the factors were varied. Nonetheless, the ranges encompass much of the variability to be found in continental margin sediments.

3. Results and discussion

3.1. N fluxes and porewater concentrations

During winter the bottom waters were well oxygenated with pronounced seasonality and severe hypoxia in late summer (Fig. 2). Nitrogenous nutrient concentrations were more variable, with higher concentrations in January than in March due to consumption during the spring bloom. The corresponding winter ex situ flux measurements of NO_3^-, NO_2^- and NH_4^+ are presented in Table 4, and showed a clear trend of NO_3^- uptake and NH_4^+ release. The mean NH_4^+ efflux (1.74 mmol m^{-2} d^{-1}) was about 5 times greater than the NO_3^- influx (−0.35 mmol m^{-2} d^{-1}). By comparison, the mean NO_2^- efflux was negligible (0.01 mmol m^{-2} d^{-1}). The net flux of DIN was 1.39 mmol m^{-2} d^{-1} and directed out of the sediment due to the large NH_4^+ efflux. The sediments were, therefore, a net source of DIN in winter. The modeled fluxes are in very close agreement with these values (Table 4). A short distance away up the channel bank (20 m water depth) the sediments are also a net source of DIN, but instead due to NO_3^- and NO_2^- efflux rather than NH_4^+ which displays a negligible flux (Balzer, 1984). At this site, the sediments are sandier, possibly more efficiently aerated, and thus favorable for nitrification. The large NH_4^+ efflux is not obvious from the NH_4^+ porewater concentration profile which is essentially vertical in the upper 10 cm and thus indicative of very low diffusive flux (Fig. 3). The concentration profiles of SO_4^{2-}, TCO_2, TA and H_2S show similar trends, all of which point toward intense bioirrigation at this site. High rates of irrigation down to 10 cm have been quantified in Boknis Eck sediments using ex situ incubations of sediment cores with bromide (Dale et al., unpublished). This non-local transport accounts for 76% of the NH_4^+ loss to the water column (Table 4).

The concentration gradients continue to evolve down through the deeper sediment layers sampled with the long core, which clearly indicates ongoing diagenesis (Fig. 4). Production of CH_4 and $CH_{4(g)}$ by the G2 and G3 fractions and their subsequent removal by AOM leads to the development of a steep change in concentration gradients of SO_4^{2-}, TCO_2, TA and CH_4 at 40 cm where the zone of anaerobic oxidation of methane by sulfate is situated (Figs. 3 and 4).

Molecular diffusion is a minor transport pathway for NO_3^- into the sediments. 76% of the NO_3^- influx is attributed to uptake by sulfide oxidizing bacteria (0.26 mmol m^{-2} d^{-1}), and irrigation accounts for 90% of the remainder (Table 4). The elevated porewater NO_3^- concentrations observed may reflect the dominance of non-local transport (Fig. 3). For example, bioirrigation may either supply NO_3^- directly or facilitate nitrification on burrow walls. Such linkages between faunal activity and the N cycle have been investigated previously (Gilbert et al., 2003; Bertics et al., 2010).

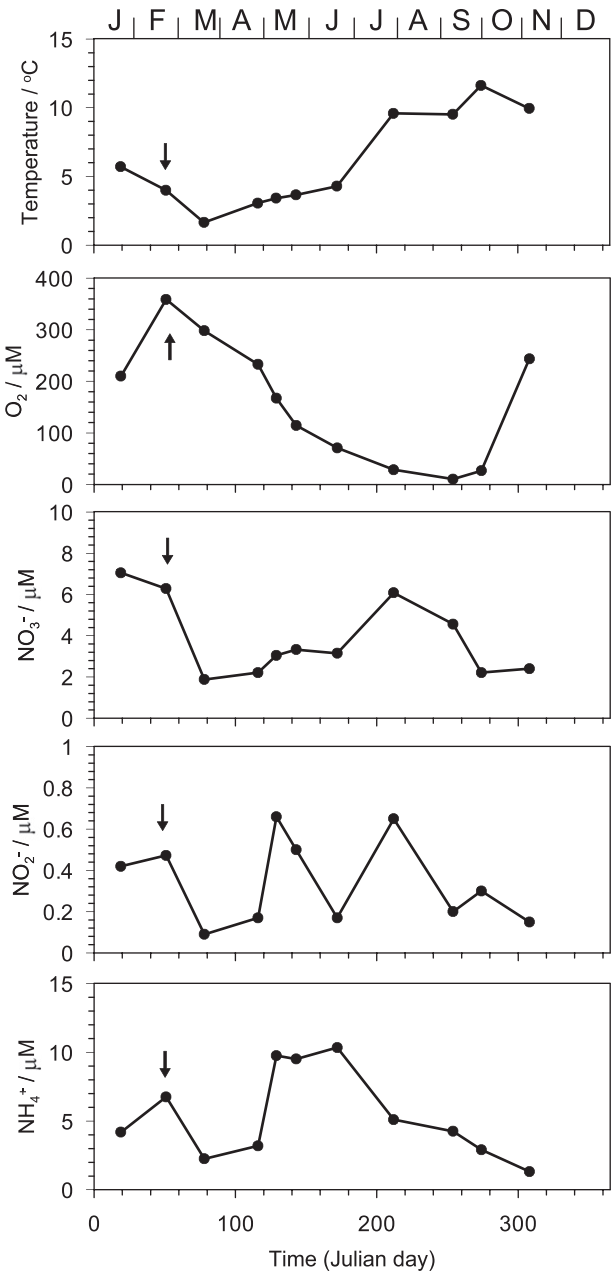

Fig. 2. Measured temperature, dissolved oxygen and nutrient concentrations at 25 m water depth at Boknis Eck during 2010 measured by the Boknis Eck Time Series project (see Acknowledgement for more information). The data marked with an arrow were measured at the time of sediment sampling, where the nutrients were measured in the supernatant of the retrieved multicores.

However, our modeled and NO_3^- penetration depths (1–2 cm) are the same as those measured previously using microbiosensors (Preisler et al., 2007), which points towards experimental artefacts rather than natural phenomena. Although we cannot be completely sure, it is likely that cell lysis due to depressurization and porewater extraction by squeezing in addition to the potential for NH_4^+ oxidation during sample manipulation are responsible for the high NO_3^- concentrations (e.g. Berelson et al., 1990; Rysgaard et al., 1994).

3.2. POC and PON mineralization

Table 5 shows the derived rate parameters for the 3 organic matter fractions in the short and long core models, in addition to

Table 4
Measured and modeled fluxes across the sediment–water interface in Boknis Eck (mmol m^{-2} d^{-1}) and the Pearson's correlation coefficient (in parenthesis). Positive and negative signs indicate efflux and influx, respectively. (DIN = NO_3^- + NO_2^- + NH_4^+).

	NO_3^-	NO_2^-	NH_4^+	DIN
18 February 2010				
Core 1	−0.44 (0.74)	+0.03 (0.61)	+1.61 (0.72)	+1.20
Core 2	−0.40 (0.92)	–	+1.91 (0.97)	+1.50
23 February 2010				
Core 1	−0.05 (0.16)[a]	+0.01 (0.63)	+0.34 (0.40)[a]	+0.30[a]
Core 2	−0.22 (0.75)	−0.02 (0.51)	+1.70 (0.97)	+1.47
Mean ex situ flux	−0.35 ± 0.12	+0.01 ± 0.02	+1.74 ± 0.15	+1.39 ± 0.16
Modeled flux	−0.34 [−0.26][b]	+0.01	+1.73	+1.40
(% by bioirrigation)	90[c]	27	76	–

[a] Not included in the calculation of mean ex situ fluxes due to low level of statistical significance.
[b] Figure in brackets is the predicted nitrate uptake by *Beggiatoa*.
[c] Not including nitrate uptake by *Beggiatoa*.

the depth integrated rates of POC mineralization and ammonification. The vast bulk of POC mineralization (97%) and ammonification (95%) rates in the upper 60 cm (short core) is due to the degradation of the reactive G1 pool. Because of the low attenuation length of G1 ($1/\gamma_{G3} = 4.3$ cm), it is almost completely degraded by 60 cm, as is further evident from the low carbon burial efficiency (CBE) of 0.5% at the same depth. By contrast, the high CBEs of the G2 and G3 fractions of 77 and 93% at 60 cm, respectively, confirm their minor degradation in the short core. Consequently, the simulated total carbon degradation rate in Fig. 5a is almost entirely due to G1.

In the long core, the slowly degrading G3 fraction accounts for a greater proportion (58%) of total mineralization than G2 (42%). The attenuation length of the G3 pool ($1/\gamma_{G3}$) is 167 cm, compared to 47 cm for G2, and so it degrades over larger depths and longer timescales. Overall, the rate of NH_4^+ production in the long core (0.56 mmol m^{-2} d^{-1}) is about half that in the short core (1.29 mmol m^{-2} d^{-1} of NH_4^+). Similarly, about one quarter of TCO_2 production occurs in the long core. Consequently, the concentration profiles solutes (NH_4^+, TCO_2, TH_2S, TA, CH_4) below the irrigation layer down to 500 cm are strongly modified by the mineralization of the G2 and G3 pools (Fig. 4), which justifies the use of fixed concentrations for their lower boundary conditions in the short core model (Fig. 3).

The depth integrated total rate of carbon degradation in the short core (14.2 mmol m^{-2} d^{-1} of C) is roughly a third of the annual mean primary production (36 mmol m^{-2} d^{-1} of C; Bodungen, 1975), reflecting the fact that most POC deposition takes place during the spring and autumn blooms (Smetacek, 1984). Our value shows a remarkably good agreement with the mean winter and spring value of 12.2 mmol m^{-2} d^{-1} of C for water depths > 14 m calculated by a carbon mass balance (Balzer et al., 1986). POC mineralization is much higher than the rate of benthic O_2 uptake (8.4 mmol m^{-2} d^{-1} of O_2) (Table 6) due of irrigation of reduced metabolites, in particular H_2S, out of the sediment before they can be oxidized. Balzer et al. (1986) measured a winter rate of 9.1 mmol m^{-2} d^{-1} of O_2 using in situ chambers, which again provides independent corroboration of our results. This value can be expected to increase to 13 mmol m^{-2} d^{-1} of O_2 following the spring bloom deposition and the ensuing enhancement of benthic activity (idem). The model predicts that 57 and 40% of POC is degraded by O_2 and SO_4^{2-}, respectively, with other mineralization pathways constituting the remaining 3% (Table 6).

It is important to note that, as with the ex situ fluxes, the high mineralization rates in the surface layers are not apparent from the geochemical solute profiles due to intense bioirrigation (Fig. 3). Irrigation has such a profound effect that the NH_4^+, TCO_2, SO_4^{2-} and TA concentration profiles cannot be used to constrain the flux and

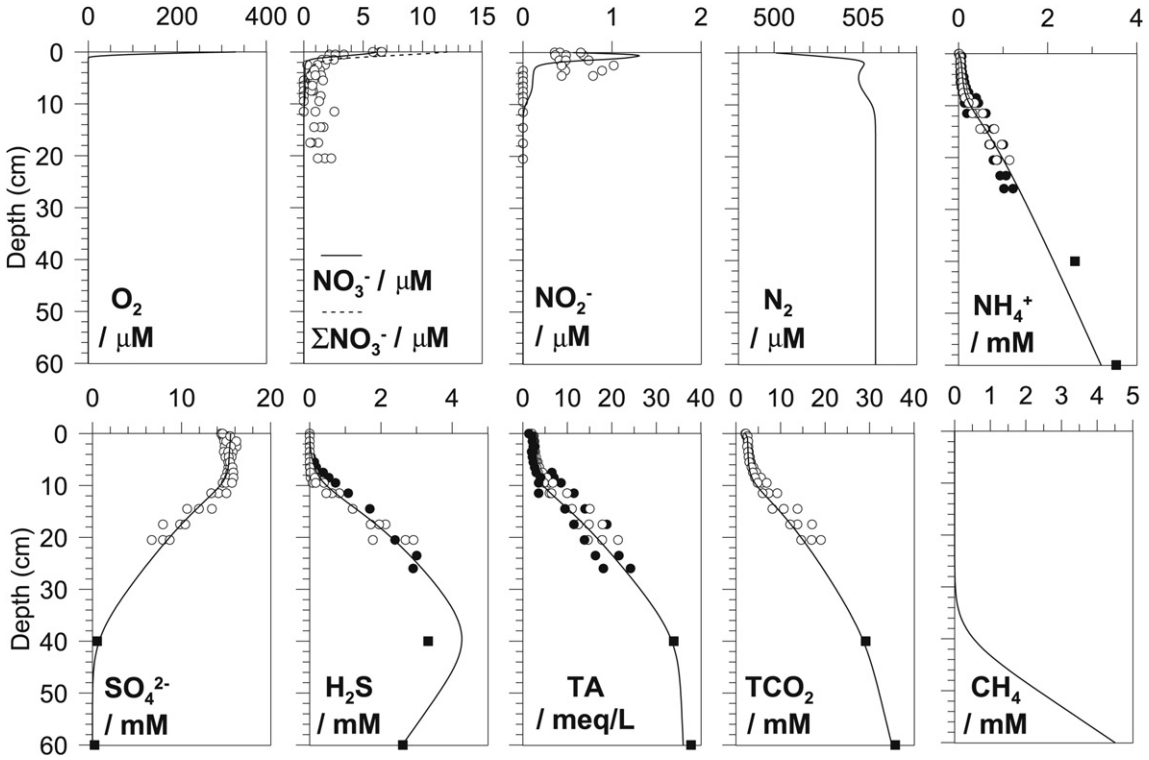

Fig. 3. Simulated (lines) and measured (symbols) geochemical depth concentration in Boknis Eck sediments. Open and closed symbols indicate that porewaters were extracted by squeezing sediments and by Rhizons, respectively. The squares correspond to measurements made in the gravity core sampled on 1 July 2010 from Fig. 4. $\Sigma NO_3^- = NO_3^- + NO_{3\,bac}^-$.

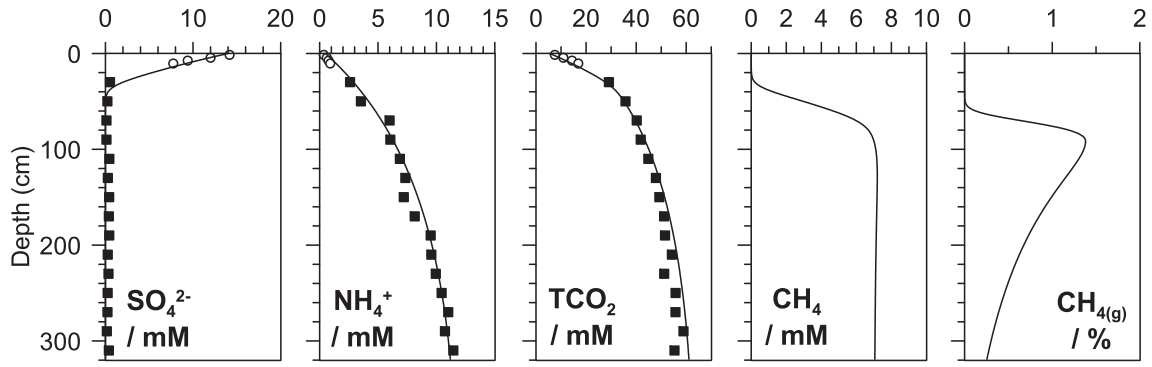

Fig. 4. Simulated (lines) and measured (symbols) geochemical depth concentration profiles in Boknis Eck sediments. The squares correspond to measurements in the gravity core sampled on 1 July 2010 and the open symbols are the mean data from Fig. 3 for comparison. Note that only the upper 300 cm are shown.

reactivity of the labile carbon pool. For this reason, the rate and depth distribution of G1 mineralization were mainly constrained using measured rates of sulfate reduction (Fig. 5b) and the NH_4^+ efflux. The slight underestimation of the modeled sulfate reduction rates in the top 5 cm is not a cause for concern when one considers that they increase to 300 nmol cm^{-3} d^{-1} of SO_4^{2-} following deposition of plankton blooms (Treude et al., 2005). The modeled rates presented here are thus good approximation of the highly contrasting pre-bloom winter situation when the mineralization rate is an order of magnitude lower.

A cautionary note must be made on the steady state assumption used to determine the fluxes and reactivity of the organic matter pools. Mineralization of G1 is certainly not constant over the year since, as mentioned above, the rate of sulfate reduction in the surface layers varies greatly between seasons due to the degradation of the spring and autumn blooms as well the effect of seasonal temperature changes of ca 10 °C on reaction rates (Treude et al., 2005). The steady state assumption is probably more applicable to the G2 and G3 pools, which are much less reactive and degrade over greater sediment depths. However, there is evidence to suggest that the system has attained a quasi steady state over winter. For example, if the reactivity of fresh organic matter degrades with a rate constant, k_f, of ca 10 yr^{-1} (Middelburg, 1989) the corresponding decay half life is $(-\ln(0.5)/k_f =)$ 25 days. Sampling took place in February 2010, which is a time difference of approximately 4–5 half–lives for fresh phytodetritus following the autumn bloom deposition which normally occurs in October (Graf et al., 1982, 1983). The autumn bloom would thus be completely degraded by February with only a few percent remaining. In fact, Meyer–Reil et al., (1987) reported that benthic metabolism decreased rapidly following the autumn bloom reaching baseline levels by December, and the same author measured low, but variable, enzymatic activities during winter (Meyer–Reil, 1983). However, persistently low winter temperatures may be a limiting factor for respiration and allow a quasi steady state may be achieved by 'winter dormancy' (Smetacek, 1985). Admittedly, intra-annual benthic metabolism in Boknis Eck sediment is dynamic, and there is some evidence to suggest that benthic bacterial numbers increase steadily in shallower sediments of the channel during winter due to accumulation of resuspended terrestrial material and refractive macrophytes (Meyer–Reil et al., 1987). Without the necessary time series data of total benthic reparation in the deep channel, it is not possible to accurately determine the error incurred by assuming steady state conditions. For the present application, we assume that the error scales quantitatively with and outbalances the uncertainty in the measured fluxes (Table 4).

Table 5
Derived rate parameters for POC degradation (Gi, $i = 1, 2, 3$), including rate at top of core ($R_{G1}(0)$ and $R_{G2,3}(b)$), depth–integrated rates ($\sum R_{Gi}$) and percentage of the total depth–integrated rate attributed to each POC fraction. Data for the depths 0–60 cm and 10–500 cm are derived from the short and long core model, respectively. Ammonium production from POM is equivalent to $\sum R_{Gi} \times (N:C)_i$. (n/a = not applicable; pool G1 was not included in the long core model).

	G1	G2	G3	Total rate
$R_{Gi}(0)$ (mmol cm^{-3} d^{-1} of TCO_2)	3.95×10^{-4}[a]	–	–	
$R_{Gi}(b)$ (mmol cm^{-3} d^{-1} of TCO_2)[b]	–	3.56×10^{-6}	1.44×10^{-6}	
γ_{Gi} (cm^{-1})	0.234[c]	0.021	0.006	
$1/\gamma_{Gi}$ (cm)	4.3	47	167	
$(N:C)_i$ (from Table 2)	9.5	8	27	
CBE at 60 cm (%)	0.5	77	93	
Short core depth-integrated rates				
$\sum R_{Gi}$ (0–60 cm) (mmol cm^{-3} d^{-1} of TCO_2)	13.7	0.3	0.1	14.2
% total	97	2	1	
$\sum R_{Gi} \times (N:C)_i$ (0–60 cm) (mmol cm^{-3} d^{-1} of NH_4^+)	1.23	0.02	0.03	1.29
% total	95	2	3	
Long core depth-integrated rates				
$\sum R_{Gi}$ (10–500 cm) (mmol TCO_2 cm^{-3} d^{-1})	n/a	1.33	1.82	3.15
% total	n/a	42	58	
$\sum R_{Gi} \times (N:C)_i$ (10–500 cm) (mmol cm^{-3} d^{-1} of NH_4^+)	n/a	0.10	0.46	0.56
% total	n/a	18	82	

[a] Derived from the short core model results as the sum of $R_{O2} + R_{NO3} + R_{NO2} + R_{Fe} + R_{SO4} + R_{CH4}$ at the sediment surface (0–1 cm).
[b] Imposed rate at sediment surface in long core model.
[c] Estimated as $k_{G1}/v_S(0)$, where $v_s(0)$ (cm d^{-1}) is the sedimentation velocity at the top of the short core (see Supplementary Material).

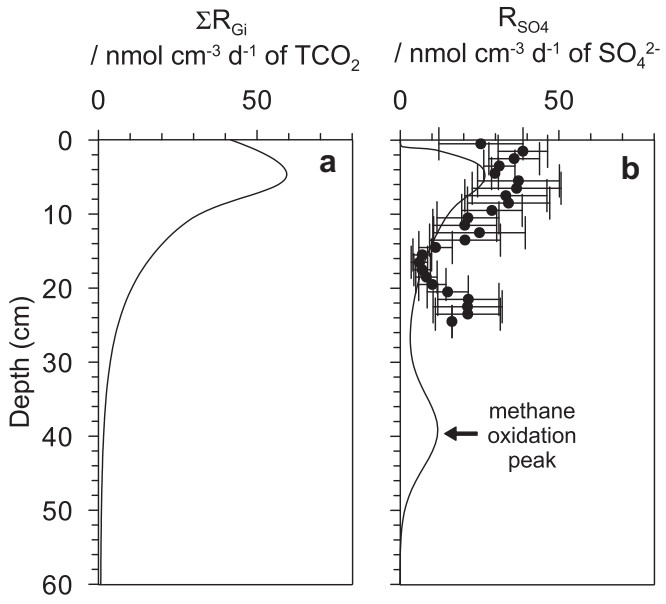

Fig. 5. (a) Simulated total organic carbon degradation rate ($\Sigma R_{Gi} = R_{O2} + R_{NO3} + R_{NO2} + R_{Fe} + R_{SO4} + R_{CH4}$, Table 1), (b) simulated (line) and measured (symbols) depth profile of the sulfate reduction rate (R_{SO4}) in Boknis Eck sediments from Treude et al. (2005). The depth of the simulated peak of anaerobic oxidation of methane is indicated.

3.3. N-turnover rates in Boknis Eck sediments during winter

The depth integrated rates of N-turnover processes in the short core that contribute to the exchange of nitrogen between the sediment and water column are listed in Table 6 by decreasing magnitude. There are no previous published studies of direct measurements of N-turnover in Boknis Eck sediments. The rates were parameterized according to a well constrained modeling study of sediments from the Peruvian OMZ by Bohlen et al. (2010), and we are fully aware that the same parameter values may not be applicable to Boknis Eck sediments. This is a shortcoming of the present study which needs to be reconciled in the future with labeling experiments. At the present time, the rates reported are theoretical yet represent our best estimate for N redox cycling pathways in Boknis Eck.

Ammonification is the most important process (1.28 mmol m^{-2} d^{-1} of NH_4^+) plus the additional 0.29 mmol m^{-2} d^{-1} of NH_4^+, which diffuses up from deeper sediments. DNRA is the next most important process quantitatively (0.26 mmol m^{-2} d^{-1}) and accounts for 20% of the NH_4^+ input. This prominent role of DNRA for N cycling is a common characteristic of coastal sediments with high carbon oxidation rates (Jørgensen and Nelson, 2004). Although *Beggiatoa* were not visible by eye on the sediment surface, they are located below the surface where they form a biological interface between the oxic and the anoxic sulfidic layers (Preisler et al., 2007). These authors measured a DNRA rate of 0.04 mmol m^{-2} d^{-1} of NH_4^+ by $^{15}NO_3^-$ incubation in Boknis Eck, which is 1 order of magnitude lower than both our modeled DRNA rate and net NH_4^+ and NO_3^- fluxes (Table 4). However, they also reported a 10 fold or more variability in *Beggiatoa* biomass between March 2002 and January 2003 which may be related to bloom deposition and very likely explains some of the divergence between our modeled and their measured rates. Nitrification (step 1) consumes only a few percent of NH_4^+ produced by these processes, which is not surprising since almost all NH_4^+ is flushed out to the seawater by irrigation. Although benthic NH_4^+ production and release increases productivity in shallow waters (An and Gardner, 2002; Dale and Prego, 2002), it remains to be shown if this export of NH_4^+ to the water column in winter is important for sustaining the spring bloom in Boknis Eck (Smetacek, 1985).

The uptake of NO_3^- from the water column by DNRA is twice as large as the loss of NO_3^- by step 1 of denitrification (0.12 mmol m^{-2} d^{-1} of NO_3^-). Furthermore, nitrification (step 2) supplies only 25% of the NO_3^- reduced by denitrification (step 1) to NO_2^-. Therefore, (i) DNRA rather than denitrification drives the flux of NO_3^- into the sediment, and (ii) the bottom water is the most important NO_3^- source for heterotrophic denitrification of NO_3^- to NO_2^-.

Denitrification (step 2) and anammox are of ecological significance since these pathways reduce NO_2^- to N_2 thereby regulating the flux of DIN to the water column. The total loss of fixed N by denitrification and anammox is 0.12 mmol m^{-2} d^{-1} of NO_2^- and is equal to 35% of the NO_3^- influx. Balzer (1984) estimated a denitrification rate of 0.34 mmol m^{-2} d^{-1} at the nearby sandy site. The total N_2 production rate reported here (0.08 mmol m^{-2} d^{-1} of N_2) is at the lower end of N_2 production rates in the Baltic Sea region (Rysgaard et al., 2001; Tuominen et al., 1998 and references therein) and other continental shelf settings (Devol, 1991; Devol and Christensen, 1993; Dale and Prego, 2002; Rysgaard et al., 2004; Glud et al., 2009). The likely explanation is that $NO_{3\,BW}^-$ in Boknis Eck (6 μM) is up to 6 fold lower than reported for these other study areas, and which may strongly limit N_2 production by denitrification and anammox (see Section 3.4). The model predicts that anammox accounts for 50% of N_2 production. However, only ca 10% is expected for Boknis Eck based on the correlation by Dalsgaard et al. (2005) between the relative contribution of anammox to N_2 production and water depth (0–800 m). As discussed in the following section, we ascribe this discrepancy to the intense irrigation in Boknis Eck sediments.

Table 6
Modeled turnover rates in the short core (0–60 cm).

Pathway	Rate	Unit
PON deposition	1.79	mmol m^{-2} d^{-1} of N
Ammonification	1.22	mmol m^{-2} d^{-1} of NH_4^+
PON burial (60 cm)	0.51	mmol m^{-2} d^{-1} of N
NH_4^+ influx across lower boundary (60 cm)	0.29	mmol m^{-2} d^{-1} of NH_4^+
DNRA	0.26	mmol m^{-2} d^{-1} of NH_4^+
Denitrification step 1: $NO_3^- \rightarrow NO_2^-$	0.11	mmol m^{-2} d^{-1} of NO_2^-
Denitrification step 2: $NO_2^- \rightarrow N_2$	0.08	mmol m^{-2} d^{-1} of NO_2^-
Nitrification step 1: $NH_4^+ \rightarrow NO_2^-$	0.06	mmol m^{-2} d^{-1} of NH_4^+
Anammox	0.04	mmol m^{-2} d^{-1} of NO_2^-
Nitrification step 2: $NO_2^- \rightarrow NO_3^-$	0.03	mmol m^{-2} d^{-1} of NO_2^-
Contribution of anammox to N_2 production	50	%
Total benthic O_2 uptake	8.4	mmol m^{-2} d^{-1} of O_2
POC mineralization by O_2	57	%
POC mineralization by SO_4^{2-}	40	%

3.4. Regulation of nitrification, denitrification, DNRA and anammox by environmental variables

To gain mechanistic insight into the processes controlling N-turnover, we developed the system analysis to identify the main environmental factors which exert the most effect on the reaction rates. Although the results are constrained using measured data from Boknis Eck, the widespread occurrence of these processes in marine sediments allows for a more general discussion. Furthermore, the transport parameters and bottom water chemistry ranges tested in the system analysis encompass much of the variability which one may encounter in continental margin settings.

The plot in Fig. 6a shows the main factors which control the rate of DNRA (R_{DNRA}). The factors which lie furthest away from the normal distribution line (dashed) are those which cause the greatest change in DNRA over the tested parameter ranges. α_{b1}, one of the parameters determining the uptake of NO_3^- by large sulfur

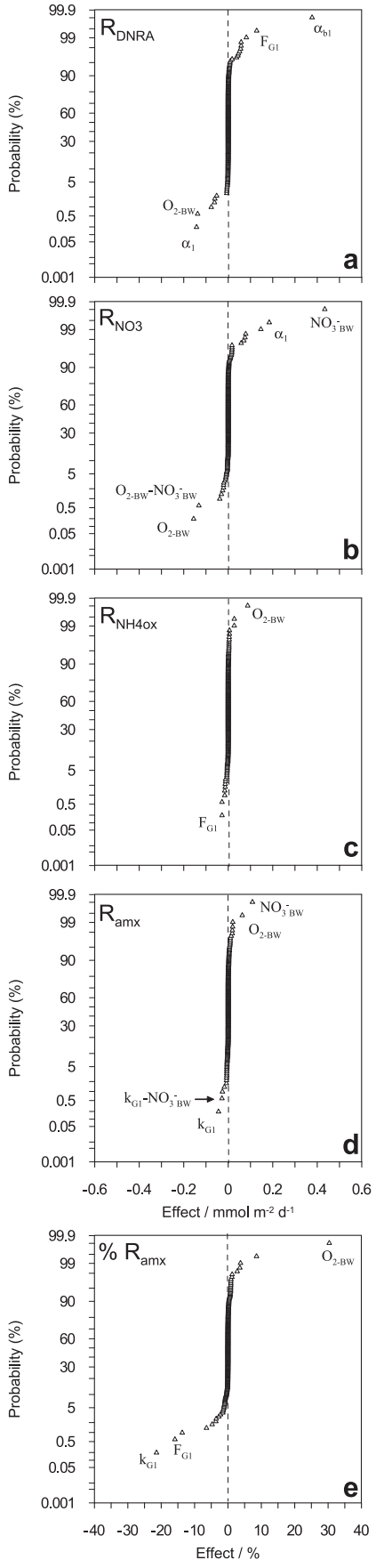

bacteria, has the largest effect on this process and lies on the right hand side of the plot. This means that an increase in α_{b1} leads to an increase in DNRA rate, by an amount equal to 0.38 mmol m^{-2} d^{-1} of NO_3^- for the tested range of α_{b1} of 0.27–1.37 d^{-1} (100–500 yr^{-1}). The interpretation here is straightforward; more intense nitrate transport enhances the rate of DNRA. In the present context, one can assume that α_{b1} is analogous to the intracellular concentration of nitrate ($NO_{3\,bac}^-$) or the biomass of sulfide oxidizing bacteria. An increase in the flux of G1, F_{G1}, also favors DNRA since this leads to higher rates of sulfide production and accumulation of free sulfide. On the other hand, the rate of irrigation by animals, α_1, and the bottom water oxygen concentration, O_{2-BW}, lie on the left hand side of the figure which indicates that an increase in these factors will tend to decrease DNRA. This arises from a greater flushing of burrows and removal of sulfide by bioirrigation (data not shown) and from aerobic sulfide oxidation. Increased ventilation further enhances aerobic oxidation of POM and, hence, reduces the rate of sulfate reduction by lowering the amount of carbon which can be oxidized by this pathway.

The system analysis results for denitrification (step 1) are shown in Fig. 6b (R_{NO3}). Essentially the same results were obtained for denitrification (step 2) (data not shown). There are 3 factors which exert most control on these processes; bottom water nitrate concentration ($NO_{3\,BW}^-$), O_{2-BW} and α_1. Higher $NO_{3\,BW}^-$ increases denitrification rates since this process is NO_3^- limited. Higher O_{2-BW} decreases denitrification because of preferential organic carbon consumption by aerobic bacteria, ultimately leading to carbon limitation for denitrification (Middelburg et al., 1996). Any potential positive feedback by higher O_{2-BW} due to coupled nitrification–denitrification is negligible by comparison. In fact, the analysis for nitrification (R_{NH4ox}, Fig. 6c) shows that the tested increase in O_{2-BW} raises nitrification by a smaller amount than it decreases denitrification (Fig. 6b).

The data point corresponding to $NO_{3\,BW}^-$ on the denitrification plot (Fig. 6b) is much further displaced from the normal distribution line than O_{2-BW}, which implies that denitrification (step 1) is much more sensitive to this variable. However, the combined effect of these parameters is also important, as can be seen by the second order interaction term O_{2-BW}–$NO_{3\,BW}^-$ indicated on the left of the figure. To interpret the effects individually, the bubble plot in Fig. 7a shows how denitrification responds to high and low levels of $NO_{3\,BW}^-$ and O_{2-BW}. The rate of denitrification changes by a factor of 7–8 when $NO_{3\,BW}^-$ increases from the low to high level and when O_{2-BW} is held constant at the low level. By contrast, the increasing oxygen levels reduce denitrification by a factor of two only, thus confirming that $NO_{3\,BW}^-$ is the major control on denitrification (step 1) when considering the annual range in parameter values. Consequently, irrigation raises denitrification via enhanced influx of NO_3^-, even though the additional input of O_2 has a negative, but smaller, feedback on denitrification (Fig. 6b).

Using a similar diagenetic model based on globally averaged data, Middelburg et al. (1996) observed that sediment denitrification was most sensitive to the fluxes of organic carbon when increased by up to a factor of 3. Our results demonstrate that carbon flux (F_{G1}) is not a sensitive factor. This does not mean that carbon is unimportant for denitrification since this has been clearly demonstrated on numerous occasions (reviewed by Dalsgaard

Fig. 6. Normal probability plots derived from the factorial analysis showing the effects of the environmental forcings on the depth integrated rates (in mmol m^{-2} d^{-1}) of (a) DNRA, (b) denitrification (step 1), (c) nitrification, (d) anammox, and (e) relative contribution of anammox to total N_2 production (in %). (a) to (d) are plotted on the same scale to facilitate comparison of the overall effects. Note that the results for denitrification (step 2) (not shown) are essentially the same as those for denitrification (step 1).

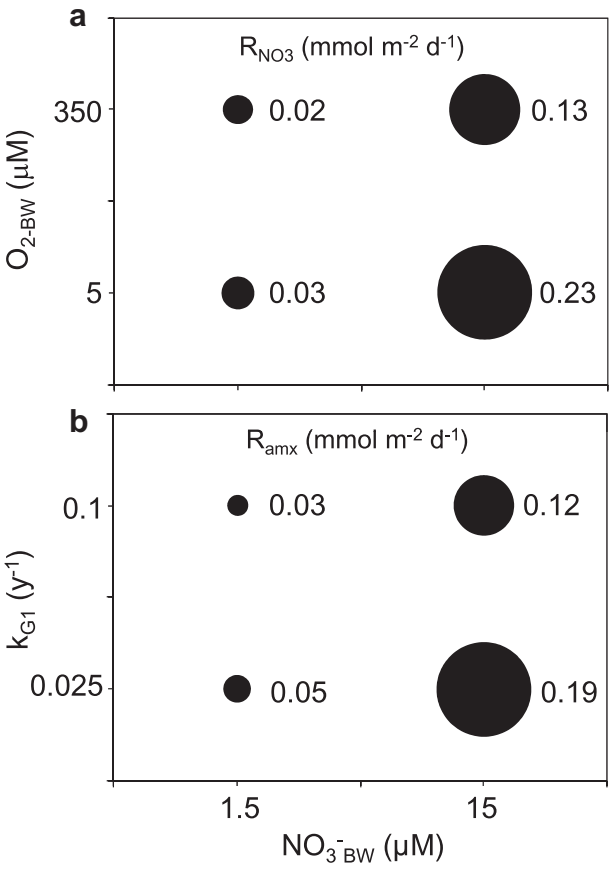

Fig. 7. Bubble plots showing the depth integrated rates of (a) denitrification (step 1), and (b) anammox due to the interaction terms between $O_{2-BW-NO3BW}$ and $k_{G1}-NO_{3\,BW}^{-}$, respectively. The axes indicate the high and low levels of the factors tested (Table 3) and the values adjacent to the bubbles are the effects of the interactions on rates (in mmol m^{-2} d^{-1}).

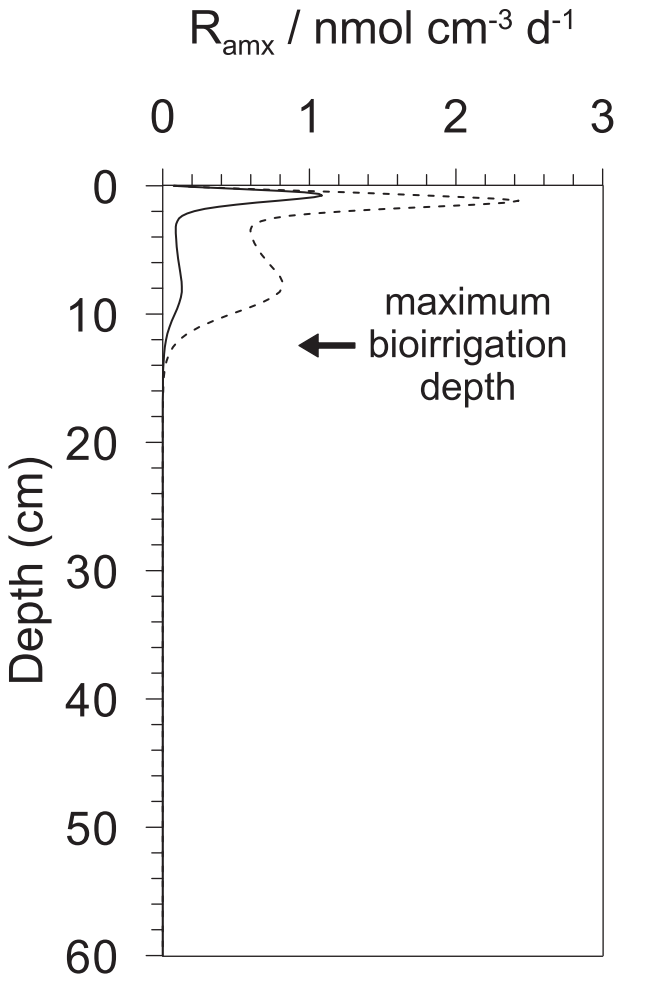

Fig. 8. Simulated rates of anammox (R_{amx}, Table 1) in Boknis Eck sediments using low (1.5 μM, solid line) and high (15 μM, dashed line) bottom water nitrate concentrations.

et al., 2005). Instead, it shows that the inter-annual variability in organic matter flux in Boknis Eck places less stringent substrate limitation constraints on denitrification than changes in bottom water chemistry. In other words, denitrification is more limited by the availability of NO_3^- than organic carbon in Boknis Eck sediments, much in the same way as the muddy sediments of the Thames estuary (Trimmer et al., 2000). This discrepancy demonstrates the need for careful consideration of site specific $NO_{3\,BW}^{-}$, O_{2-BW} and carbon oxidation rates when estimating regional or global benthic N budgets, especially in coastal sediments where spatial heterogeneity in turnover rates tends to be much larger than in slope or abyssal sediments.

The results for anammox (R_{amx}) reveal that increased levels of $NO_{3\,BW}^{-}$ and O_{2-BW} lead to higher rates, whereas increased reactivity of G1 (k_{G1}) has the opposite effect (Fig. 6d). Overall, $NO_{3\,BW}^{-}$ and k_{G1} have the largest single effects, yet these terms also weakly interact ($k_{G1}-NO_{3\,BW}^{-}$). As for denitrification, further examination shows that anammox is far more sensitive to $NO_{3\,BW}^{-}$ than k_{G1} (Fig. 7b). The importance of $NO_{3\,BW}^{-}$ on anammox arises through the production of NO_2^- ($NO_3^- \rightarrow NO_2^-$) by denitrification (step 1).

To illustrate this effect, Fig. 8 shows the modeled rate of anammox with low (1.5 μM) and high (15 μM) $NO_{3\,BW}^{-}$, with all other parameters unchanged. It is clear from the figure that higher $NO_{3\,BW}^{-}$ greatly stimulates anammox in the subsurface irrigated layers by alleviating NO_2^- limitation of ammonium oxidizers. Irrigated sediments have a large capacity for N redox cycling due to the increased effective surface area of the sediment by burrow walls (Aller et al., 1983), and we conclude that deep NO_3^- transport and reduction gives rise to the elevated relative importance of anammox to N_2 production estimated for Boknis Eck (50%, Table 6). Enhanced transport of NO_3^-, and thus NO_2^-, to sediment layers where anammox is NO_2^- limited establishes a critical linkage between denitrification, anammox and biota and may provide an explanation for the observed strong correlation between anammox and $NO_{3\,BW}^{-}$ (Risgaard–Petersen et al., 2004; Rysgaard et al., 2004; Trimmer et al., 2003).

O_{2-BW} also enhances anammox since it leads to higher rates of nitrification (Fig. 6c,d) but, as mentioned, its effect is less important than $NO_{3\,BW}^{-}$. On the other hand, higher O_{2-BW} greatly enhances the relative importance of anammox to total N_2 production, % R_{amx} (Fig. 6e). This implies that coupling of anammox and nitrification ($NH_4^+ \rightarrow NO_2^-$) leads to high % R_{amx}, whereas coupling of anammox and denitrification ($NO_3^- \rightarrow NO_2^-$) favors higher absolute rates of anammox. Consequently, % R_{amx} is strongly yet negatively affected by k_{G1} because higher carbon reactivity channels more O_{2-BW} into mineralization at the expense of nitrification and increases the demand on NO_2^- by denitrification (step 2) (Trimmer and Nicholls, 2009). In fact, nitrification responds negatively to increased carbon fluxes (Fig. 6c). We thus propose that this explains why absolute and relative rates of anammox are generally inversely correlated (Dalsgaard et al., 2005), that is, because the controls on NO_2^- sources (i.e. nitrification and denitrification) are different and vary in intensity depending on the type of setting (see Section 3.5).

3.5. Synthesis: biogeography of denitrification, DNRA and anammox

The system analysis shows that the environmental factors which exert a major control on N-turnover processes are also those which display high variability in natural settings. This allows us to broadly summarize the types of environment where the relative importance of DNRA, denitrification and anammox are highest.

It is well known that sediments in upwelling regions, oxygen minimum zones and hypoxic basins and bays tend to be colonized by mats of large sulfur bacteria and exhibit high rates of DNRA (e.g. Fossing et al., 1995; Preisler et al., 2007). Yet, Jørgensen and Nelson (2004) postulate that their occurrence is widespread in coastal sediments such as Boknis Eck which receive high fluxes of phytodetritus even though bottom waters are permanently or seasonally oxic. However, because the half saturation constant of NO_3^- for denitrification is much lower than that for DNRA (10^1 versus 10^2 uM; Tiedje et al., 1982), denitrifiers should, in theory, strongly compete or even outcompete sulfide oxidizers for bottom water NO_3^-. Nonetheless, filamentous motile sulfide oxidizers such as *Beggiatoa* and *Thioploca* have a physiological advantage over denitrifying bacteria since they can access the seawater NO_3^- reservoir directly by extension of their filaments through the diffusive boundary layer into the water column (e.g. Huettel et al., 1996). Denitrifying bacteria will be limited by NO_3^- transport into the sediment by diffusion. Therefore, they do not strictly compete with each other for NO_3^-. The versatility of motile sulfur bacteria to access seawater NO_3^- is undoubtedly one reason why DNRA is a major pathway in N cycling even in coastal sediments provided that the organic matter loading is high enough (reviewed by Jørgensen and Nelson, 2004). Note, however, that non-filamentous sulfide oxidizers such as the giant non-motile *Thiomargarita* also rely on molecular diffusion or resuspension of surface sediments to access the seawater NO_3^- reservoir (Schulz and Jørgensen, 2001). Toxicity toward sulfide may also be a limiting factor for denitrifying bacteria in these environments (Sørensen et al., 1987), although this was not explicitly included in the model presented here.

Given that free sulfide accumulation in the porewater is a prerequisite for giant sulfur bacteria, we should expect to find a reduction in the dominance of DNRA as carbon flux decreases. Denitrification should then take over as the major consumer of bottom water NO_3^- when a tipping point in carbon flux and/or reactivity has been reached. In support of this thesis, benthic data collected recently along the 11 °S transect of the Peruvian OMZ do in fact show that the relative importance of denitrification to total NO_3^- uptake increases steadily from ca 23% on the shelf where carbon concentrations are ca 10 wt.%, to ca 100% on the continental slope where carbon concentrations are 4 wt.% and bottom water oxygen was 40 μM (Bohlen et al., 2010). Seafloor observations further reveal that sulfide oxidizing bacteria are present at high densities on the Peruvian shelf (Levin et al., 2002). An increase in denitrification at the expense of DNRA has also been observed with increasing distance away from caged fish farms, which illustrates that the same tendencies also operate over much smaller spatial scales (Christensen et al., 2000). These studies suggest that it is the dynamic interplay between carbon flux and reactivity (hence sulfide concentration) and oxygen availability that determines whether the sediments will be net recyclers (i.e. by DNRA) or sinks (i.e. by denitrification) of DIN.

Our analysis has highlighted a potentially critical role of nitrification in supporting high relative rates of N_2 production by anammox (% R_{amx}) and of denitrification in supporting high absolute rates of anammox (R_{amx}). This theory fits with the data presented in the seminal study of Dalsgaard et al. (2005) and expands on their idea that $\%R_{amx}$ is negatively correlated with sediment mineralization rates. High mineralization rates invariably imply high rates of NO_2^- production by denitrification, a minor fraction of which is lost to anammox. Thus, denitrification and anammox appear to be correlated in organic-rich shallow water settings such as fjords and estuaries, but $\%R_{amx}$ remains low (Dalsgaard et al., 2005). Oxygen penetration also tends to be low in highly reactive sediments which limits the efficiency of nitrification as the other supply pathway of NO_2^- for anammox.

Anammox ought to dominate over denitrification in less reactive sediments where nitrification is maximized, such as hemipelagic continental shelf sediments. Dominance of nitrification over denitrification in these environments is evident from the fact that NO_3^- fluxes tend to be greater than NH_4^+ fluxes and directed out of the sediment (e.g. Middelburg et al., 1996; Christensen et al., 1987; Devol and Christensen, 1993). Whilst there are still very few studies which have systematically investigated denitrification and anammox in open ocean continental shelf sediments, the study by Trimmer and Nicholls (2009) is exceptional. They observed an increase in $\%R_{amx}$ from 33% on the continental shelf to 65% on the slope, which fits with the general trend compiled from individual study sites (Dalsgaard et al., 2005). With the advent of NO_3^- microbiosensors which can be deployed in situ (Glud et al., 2009), the technology is now available to more accurately quantify and correlate nitrification and anammox rates for sediments from the shelf down to the continental slope.

4. Conclusions

This study aims to understand the major environmental controls on N turnover processes in surface marine sediments of Boknis Eck; a seasonally hypoxic channel in the SW Baltic Sea. The results of a numerical model are confirmed using field data including porewater geochemistry and measured fluxes across the seafloor. Boknis Eck sediments are reactive and constitute a large source of NH_4^+ due to intense irrigation of the surface sediments by indwelling macrofauna. An additional flux of NH_4^+ by *Beggiatoa* carrying out dissimilatory nitrate reduction to ammonium is also consistent with our field observations. The modeling study also provided first estimates of N turnover rates by denitrification and anammox in Boknis Eck sediments which now require experimental verification. Future work will explore how these trends behave during the transitional period to severe hypoxia, or even anoxia, which occurs at the study site in late summer.

From a systematic analysis of the model output after varying key parameters over ranges exemplary of continental margin marine sediments, we conclude that the biogeography of microbial N turnover pathways has the potential to be predicted based on the type of setting studied. For example, we hypothesize that anammox is mainly coupled to (i) denitrification in highly reactive poorly ventilated sediments (e.g. organic-rich coastal settings) and (ii) nitrification in lesser reactive yet well ventilated sediments where nitrite production and availability is maximized (e.g. hemipelagic settings). Consequently, simultaneous quantification of the rates of denitrification and nitrification are needed to understand how anammox varies over regional scales. This information is also urgently needed to quantify N fluxes in marine sediments using dynamic models and also to predict how these fluxes may change in the future due to natural and/or anthropogenic interferences.

Acknowledgements

We thank B. Domeyer, A. Bleyer, R. Surberg, R. Ebbinghaus and M. Dibbern, for the biogeochemical analyses and the crews of RV Alkor, Littorina and PolarFuchs for assistance during fieldwork. Two reviewers provided constructive comments, and we would like to

extend our thanks to the journal editor Eric Wolanski for ensuring a swift peer review of our paper. This work is a contribution of the EU–funded project Hypox (EC Grant 226213, www.hypox.net) and has received additional support from the Deutsche Forschungsgemeinschaft (DFG) through the SFB 754 "Climate–Biogeochemistry Interactions in the Tropical Ocean" (www.sfb754.de). The Boknis Eck Time Series Station is run by the Forschungsbereich Marine Biogeochemie of the IFM–GEOMAR, Kiel: http://www.ifm-geomar.de/index.php?id=bokniseck.

Appendix. Supplementary data

Supplementary data associated with this article can be found, in the online version, at doi:10.1016/j.ecss.2011.05.016.

References

Aller, R.C., Yingst, J.Y., Ullman, W.J., 1983. Content Comparative biogeochemistry of water in intertidal Onuphis (polychaeta) and Upogebia (crustacea) burrows: temporal patterns and causes. Journal of Marine Research 41, 571–604.

An, S., Gardner, W.S., 2002. Dissimilatory nitrate reduction to ammonium (DNRA) as a nitrogen link, versus denitrification as a sink in a shallow estuary (Laguna Madre/Baffin Bay, Texas). Marine Ecology Progress Series 237, 41–50.

Balzer, W., 1984. Organic matter degradation and biogenic element cycling in a nearshore sediment (Kiel Bight). Limnology and Oceanography 29, 1231–1246.

Balzer, W., Erlenkeuser, H., Hartmann, P.J., Müller, P.J., Pollehne, F., 1987. Diagenesis and exchange processes at the benthic boundary. In: Rumohr, J., Wlager, E., Zeitzschel, B. (Eds.), Seawater–Sediment Interactions in coastal Waters. An Interdisclipinary Approach, pp. 111–161.

Balzer, W., Pollehne, F., Erlenkeuser, H., 1986. Cycling of organic carbon in a coastal marine system. In: Sly, P.G. (Ed.), Sediments and Water Interactions. Springer Verlag, New York, pp. 325–330.

Berelson, W.M., Hammond, D.E., O'Neil, D., Xu, X.M., Chin, C., Zukin, J., 1990. Benthic fluxes and pore water studies from sediments of the central equatorial north Pacific: nutrient diagenesis. Geochimica et Cosmochimica Acta 54, 3001–3012.

Berelson, W.M., McManus, J., Coale, K.H., Johnson, K.S., Kilgore, T., Burdige, D., Pilskaln, C., 1996. Biogenic matter diagenesis on the sea floor: a comparison between two continental margin transects. Journal of Marine Research 54, 731–762.

Berner, R.A., 1964. An idealized model of dissolved sulfate distribution in recent sediments. Geochimica et Cosmochimica Acta 28, 1497–1503.

Berner, R.A., 1980. Early Diagenesis: A Theoretical Approach. Princeton University Press, Princeton, 241 pp.

Bertics, V.J., Sohm, J.A., Treude, T., Chow, C.E.T., Capone, D.G., Fuhrman, J.A., Ziebis, W., 2010. Burrowing deeper into benthic nitrogen cycling: the impact of bioturbation on nitrogen fixation coupled to sulfate reduction. Marine Ecology Progress Series 409, 1–15.

Bodungen, B.v., 1975. Der Jahresgang der Nährsalze und der Primärproduktion des Planktons in der Kieler Bucht unter Berücksichtigung der Hydrographie. Ph.D. thesis, Universitiy of Kiel. 116 pp.

Bohlen, L., Sommer, S., Dale, A.W., Hensen, C., Wallmann, K., 2010. Sediments underlying the Peruvian oxygen minimum zone – source or sink for reactive nitrogen species? Eos Transactions of the American Geophysical Union 91 (26) Ocean Sciences meeting Supplement, IT15D–03.

Boudreau, B.P., 1997. Diagenetic Models and Their Implementation: Modelling Transport and Reactions in Aquatic Sediments. Springer–Verlag, Berlin, 414 pp.

Box, G.E.P., Hunter, W.G., Hunter, J.S., 1978. Statistics for Experimenters. An Introduction to Design, Data Analysis and Model Building. Wiley, New York, 653 pp.

Brandes, J.A., Devol, A.H., 2002. A global marine-fixed nitrogen isotopic budget: implications for holocene nitrogen cycling. Global Biogeochemical Cycles 16, 1120. doi:10.1029/2001GB001856.

Christensen, J.P., Smethie Jr., W.M., Devol, A.H., 1987. Benthic nutrient regeneration and denitrification on the Washington continental shelf. Deep-Sea Research 34, 1027–1047.

Christensen, P.B., Rysgaard, S., Sloth, N.P., Dalsgaard, T., Schwärter, S., 2000. Sediment mineralization, nutrient fluxes, denitrification and dissimilatory nitrate reduction to ammonium in an estuarine fjord with sea cage trout farms. Aquatic Microbial Ecology 21, 73–84.

Codispoti, L.A., 1995. Is the ocean losing nitrate. Nature 376, 724.

Codispoti, L.A., Brandes, J.A., Christensen, J.P., Devol, A.H., Naqvi, S.W.A., Paerl, H.W., Yoshinari, T., 2001. The oceanic fixed nitrogen and nitrous oxide budgets: moving targets as we enter the anthropocene? Scientia Marina 65, 85–105.

Dale, A.W., Aguilera, D.R., Regnier, P., Fossing, H., Knab, N.J., Jorgensen, B.B., 2008b. Seasonal dynamics of the depth and rate of anaerobic oxidation of methane in Aarhus Bay (Denmark) sediments. Journal of Marine Research 66, 127–155.

Dale, A.W., Prego, R., 2002. Physico–biogeochemical controls on benthic–pelagic coupling of nutrient fluxes and recycling in a coastal upwelling system. Marine Ecology Progress Series 235, 15–28.

Dale, A.W., Regnier, P., Knab, N.J., Jorgensen, B.B., Van Cappellen, P., 2008a. Anaerobic oxidation of methane (AOM) in marine sediments from the Skagerrak (Denmark): II. Reaction–transport modelling. Geochimica et Cosmochimica Acta 72, 2880–2894.

Dale, A.W., Regnier, P., Van Cappellen, P., 2006. Bioenergetic controls on anaerobic oxidation of methane (AOM) in coastal marine sediments: a theoretical analysis. American Journal of Science 306, 246–294.

Dalsgaard, T., Thamdrup, B., Canfield, D.E., 2005. Anaerobic ammonium oxidation (anammox) in the marine environment. Research in Microbiology 156, 457–464.

Devol, A.H., 1991. Direct measurement of nitrogen gas fluxes from continental shelf sediments. Nature 349, 319–321.

Devol, A.H., Christensen, J.P., 1993. Benthic fluxes and nitrogen cycling in sediments of the continental margin of the eastern North Pacific. Journal of Marine Research 51, 345–372.

Dunn, R.J.K., Welsh, D.T., Jordan, M.A., Teasdale, P.R., Lemckert, C.J., 2009. Influence of natural amphipod (Victoriopisaaustraliensis) (Chilton, 1923) population densities on benthic metabolism, nutrient fluxes, denitrification and DNRA in sub–tropical estuarine sediment. Hydrobiologia 628, 95–109.

Fossing, H., Gallardo, V.A., Jørgensen, B.B., Hüttel, M., Nielsen, L.P., Schulz, H., Canfield, D.E., Glud, R.N., Gundersen, J.K., Küver, J., Ramsing, N.B., Teske, A., Thamdrup, B., Ulloa, O., 1995. Concentration and transport of nitrate by the mat–forming sulphur bacterium Thioploca. Nature 274, 713–715.

Galloway, J.N., 2003. The global nitrogen cycle. In: Holland, H.D., Turekian, K.K. (Eds.), Treatise on Geochemistry, vol. 8. Elsevier, Amsterdam, pp. 557–583.

Gilbert, F., Aller, R.C., Hulth, S., 2003. The influence of macrofaunal burrow spacing and diffusive scaling on sedimentary nitrification and denitrification: an experimental simulation and model approach. Journal of Marine Research 61, 101–125.

Glud, R.N., Thamdrup, B., Stahl, H., Wenzhoefer, F., Glud, A., Nomaki, H., Oguri, K., Revsbech, N.P., Kitazato, H., 2009. Nitrogen cycling in a deep ocean margin sediment (Sagami Bay, Japan). Limnology and Oceanography 54, 723–734.

Graf, G., Bengtsson, W., Diesner, U., Schulz, R., Theede, H., 1982. Benthic response to sedimentation of a spring phytoplankton bloom: process and budget. Marine Biology 245, 201–208.

Graf, G., Schulz, R., Peinert, R., Meyer–Reil, L.A., 1983. Benthic response to sedimentation events during autumn to spring at a shallow–water station in the Western Kiel Bight. Marine Biology 77, 235–246.

Grasshoff, K., Ehrhardt, M., Kremmling, K., 1983. Methods of seawater analysis. Verlag Chemie, Weinheim, p. 419.

Gruber, N., 2008. The marine nitrogen cycle: overview and challenges. In: Capone, D.G., Bronk, D.A., Mulholland, M.R., Carpenter, E.J. (Eds.), Nitrogen in the Marine Environment, second ed., pp. 1–50.

Gruber, N., Sarmiento, J.L., 1997. Global patterns of marine nitrogen fixation and denitrification. Global Biogeochemical Cycles 11, 235–266.

Hansen, H.P., 1993. Saisonale und langzeitliche Veränderungen chemisch–hdyrographischer parameter in der Kieler Bucht. Berichte aus dem Institut für Meereskunde 240, 2–31 (in German).

Hansen, H.P., 1999. Determination of oxygen. In: Grasshoff, K., Kremling, K., Ehrhardt, M. (Eds.), Methods of seawater analysis, third ed. Wiley, New York, pp. 75–89.

Hansen, H.P., Giesenhagen, H.C., Behrends, G., 1999. Seasonal and long-term control of bottom water oxygen deficiency in a stratified shallow-coastal system. ICES Journal of Marine Science 56 (Supplement), 65–71.

Hansen, H.P., Koroleff, F., 1999. Determination of nutrients. In: Grasshoff, K., Kremling, K., Ehrhardt, M. (Eds.), Methods of seawater analysis, third ed. Wiley, New York, pp. 159–228.

Hedges, J.I., Keil, R.G., 1995. Sedimentary organic matter preservation: an assessment and speculative synthesis. Marine Chemistry 49, 81–115.

Huettel, M., Forster, S., Kloser, S., Fossing, H., 1996. Vertical migration in the sediment-dwelling sulfur bacteria *Thioploca* spp. in overcoming diffusion limitations. Applied and Environmental Microbiology 62, 1863–1872.

Hulth, S., Aller, R.C., Gilbert, F., 1999. Coupled anoxic nitrification/manganese reduction in marine sediments. Geochimica et Cosmochimica Acta 63, 49–66.

Jørgensen, B.B., Nelson, D.C., 2004. Sulfide oxidation in marine sediments: geochemistry meets microbiology. In: AmendJ.P., EdwardsK.J., LyonsT.W. (Eds.), Sulfur Biogeochemistry—Past and Present. Geological Society of America Special Paper, 379, pp. 63–81.

Levin, L., Gutiérrez, D., Rathburn, A., Neira, C., Sellanes, J., Muñoz, P., Gallardo, V., Salamanca, M., 2002. Benthic processes on the Peru margin: a transect across the oxygen minimum zone during the 1997–98 El Niño. Progress in Oceanography 53, 1–27.

Meyer–Reil, L.A., 1983. Benthic response to sedimentation events during autumn to spring at a shallow water station in the Western Kiel Bight. Marine Biology 77, 247–256.

Meyer–Reil, L.A., Faubel, A., Graf, G., Thiel, H., 1987. Aspects of benthic community structure and metabolism. In: Rumohr, J., Wlager, E., Zeitzschel, B. (Eds.), Seawater–Sediment Interactions in coastal Waters. An Interdisclipinary Approach, pp. 69–110.

Middelburg, J.J., 1989. A simple rate model for organic matter decomposition in marine sediments. Geochimica et Cosmochimica Acta 53, 1577–1581.

Middelburg, J.J., Soetaert, K., Herman, P.M.J., Heip, C.H.R., 1996. Denitrification in marine sediments: a model study. Global Biogeochemical Cycles 10, 661–673.

Mogollón, J.M., L'Heureux, I., Dale, A.W., Regnier, P., 2009. Methane gas–phase dynamics in marine sediments: a model study. American Journal of Science 309, 189–220.

Nittrouer, C.A., Lopez, G.R., Wright, D., Bentley, S.J., D'Andrea, A.F., Friedrichs, C.T., Craig, N.I., Sommerfield, C.K., 1998. Oceanographic processes and the preservation of sedimentary structure in Eckernförde Bay, Baltic Sea. Continental Shelf Research 18, 1689–1714.

Orsi, T.H., Werner, F., Milkert, D., Anderson, A.L., Bryant, W.R., 1996. Environmental overview of Eckernförde bay, northern Germany. Geo–Marine Letters 16, 140–147.

Otte, S., Kuenen, J.G., Nielsen, L.P., Paerl, H.W., Zopfi, J., Schulz, H.N., Teske, A., Strotmann, B., Gallardo, V.A., Jørgensen, B.B., 1999. Nitrogen, carbon, and sulfur metabolism in natural *Thioploca* samples. Applied and Environmental Microbiology 65, 3148–3157.

Preisler, A., de Beer, D., Lichtschlag, A., Lavik, G., Boetius, A., Jørgensen, B.B., 2007. Biological and chemical sulfide oxidation in a Beggiatoa inhabited marine sediment. The ISME Journal 1, 341–353.

Risgaard–Petersen, N., Meyer, R.L., Schmid, M., Jetten, M.S.M., Enrich–Past, A., Rysgaard, S., Revsbech, N.P., 2004. Anaerobic ammonium oxidation in an estuarine sediment. Aquatic Microbial Ecology 36, 293–304.

Ruttenberg, K.C., 2003. The global phosphorus cycle. In: Holland, H.D., Turekian, K.K. (Eds.), Treatise on Geochemistry, vol. 8. Elsevier, Amsterdam, pp. 585–643.

Rysgaard, S., Glud, R.N., Risgaard–Petersen, N., Dalsgaard, T., 2004. Denitrification and anammox activity in Arctic marine sediments. Limnology and Oceanography 49, 1493–1502.

Rysgaard, S., Kühl, M., Glud, R.N., Hansen, J.W., 2001. Biomass, production and horizontal patchiness of sea ice algae in a high–Arctic fjord (Young Sound, NE Greenland). Marine Ecology Progress Series 223, 15–26.

Rysgaard, S., Risgaard–Petersen, N., Sloth, N.P., Jensen, K., Nielsen, L.P., 1994. Oxygen regulation of nitrification and denitrification in sediments. Limnology and Oceanography 39, 1643–1652.

Schulz, H.N., Jørgensen, B.B., 2001. Big bacteria. Annual Review of Microbiology 55, 105–137.

Schlüter, M., Sauter, E., Hansen, H.P., Suess, E., 2000. Seasonal variations of bio-irrigation in coastal sediments: modelling of field data. Geochimica et Cosmochimica Acta 64, 821–834.

Smetacek, V., 1984. Seasonal stages characterizing the annual cycle of an inshore pelagic system. In: Rapports et Proces–Verbaux des Reunions (Conseil Permanent International pour l'Exploration de la Mer), 183, pp. 126–135.

Smetacek, V., 1985. The annual cycle of Kiel bight plankton: a long–term analysis. Estuaries 8, 145–157.

Sørensen, J., Rasmussen, L.K., Koike, I., 1987. Micromolar sulfide concentrations alleviate acetylene blockage of nitrous oxide reduction by denitrifying Pseudomonas fluorescens. Canadian Journal of Microbiology 33, 1001–1005.

Straub, K.L., Benz, M., Schink, B., Widdel, F., 1996. Anaerobic, nitrate-dependent microbial oxidation of ferrous iron. Applied and Environmental Microbiology 62, 1458–1460.

Tiedje, J.M., Sexstone, A.J., Myrold, D.D., Robinson, J.A., 1982. Denitrification: ecological niches, competition and survival. Antonie Van Leewenhoek 48, 569–583.

Thamdrup, B., Dalsgaard, T., 2002. Production of N_2 through anaerobic ammonium oxidation coupled to nitrate reduction in marine sediments. Applied and Environmental Microbiology 68, 1312–1318.

Thullner, M., Dale, A.W., Regnier, P., 2009. Global-scale quantification of mineralization pathways in marine sediments: a reaction–transport modeling approach. Geochemistry, Geophysics,. Geosystems 10, Q10012. doi:10.1029/2009GC002484.

Treude, T., Krüger, M., Boetius, A., Jørgensen, B.B., 2005. Environmental control on anaerobic oxidation of methane in the gassy sediments of Eckernförde Bay (German Baltic). Limnology and Oceanography 50, 1771–1786.

Trimmer, M., Nedwell, D.B., Sivyer, D.B., Malcolm, S.J., 2000. Seasonal benthic organic matter mineralisation measured by oxygen uptake and denitrification along a transect of the inner and outer River Thames estuary, UK. Marine Ecology Progress Series 197, 103–119.

Trimmer, M., Nicholls, J.C., 2009. Production of nitrogen gas via anammox and denitrification in intact sediment cores along a continental shelf to slope transect in the North Atlantic. Limnology and Oceanography 54, 577–589.

Trimmer, M., Nicholls, J.C., Deflandre, B., 2003. Anaerobic ammonium oxidation measured in sediments along the Thames Estuary, United Kingdom. Applied and Environmental Microbiology 69, 6447–6454.

Tuominen, L., Heinänen, A., Kuparinen, J., Nielsen, L.P., 1998. Spatial and temporal variability of denitrification in the sediments of the northern Baltic Proper. Marine Ecology Progress Series 172, 13–24.

Whiticar, M.J., 1982. Determination of interstitial gases and fluids in sediment collected with an "in situ" sampler. Analytical Chemistry 54, 1796–1798.